Intended for

GSI Water Solutions Inc. for
Santa Barbara County Public Works Department Water Resources Division

Document type

Report

Date

August 2021

SANTA YNEZ EASTERN MANAGEMENT AREA GEOPHYSICAL INVESTIGATION

RAMBOLL Bright ideas. Sustainable change.

SANTA YNEZ EASTERN MANAGEMENT AREA
GEOPHYSICAL INVESTIGATION

Project name	**Santa Ynez Eastern Management Area – Processing and Inversion of AEM and tTEM Data**
Project no.	**1690017816**
Document type	**Report**
Version	**1**
Date	**August 19, 2021**
Prepared by	**Geophysicist, Max Halkjær (Ramboll)**
Checked by	**Geophysicist, Peter Thomsen (Ramboll)**
Approved by	**Geophysicist, Max Halkjær (Ramboll)**
Description	**[Text]**
Front Page	The SkyTEM AEM system flying with the sensor at low altitude within the Santa Ynez Eastern Management Area.

Ramboll
2200 Powell Street
Suite 700
Emeryville, CA 94608
United States of America

https://ramboll.com

Rambøll Danmark A/S
DK reg.no. 35128417

Member of FRI

WATER

GSI Water Solutions Inc. for
Santa Barbara County Public Works Department
Water Resources Division

Santa Ynez Eastern Management Area – Geophysical Investigation

August 23, 2021

To Whom it May Concern,
Ramboll is pleased to submit this report of the study conducted for GSI Water Solutions Inc. for Santa Barbara County Public Works Department Water Resources Division.

The study area is geographically located within the groundwater basin Santa Ynez River Valley number 3-015 Eastern Management Area. Two geophysical investigation methods, towed- transient electromagnetic (tTEM) surveying and airborne electromagnetic (AEM) surveying, was been applied to provide more information about the geology in the basin.

The report covers the following activities: AEM survey planning; Data gathering, Quality Control of the data; Processing and Inversion; and Presentation and reporting of the data. The report does not include documentation for the calibration of the AEM system and the basic configuration of the AEM system as this information has been described in a separate report by SkyTEM Surveys APS. The geologic and hydrogeological interpretation is described briefly to create a basis that can be applied across the entire basin.

We appreciate the staff from GSI Water Solutions Inc for their support during the survey design and field operation. We will remain available at your convenience to discuss this report or to answer any questions.

Yours sincerely

Ramboll
2200 Powell Street
Suite 700
Emeryville, CA 94608
United States of America

Ahmad Ali Behroozmand
Geophysicist
Ramboll Water Resources

D +1 510-420-2580
abehroozmand@ramboll.com

Max Halkjær
Market Manager, Hydrogeologist, Geophysicist
Ramboll Water Resources

M +45 51 61 29 60
maxh@ramboll.com

CONTENTS

TABLE OF FIGURES

TABLE OF TABLES

APPENDICES

Appendix 1
AEM Processing and Inversion Settings

Appendix 2
TTEM Instrumentation, Processing and Inversion Settings

Appendix 3
AEM Mean Resistivity Maps – 20 Meter Elevation Intervals

Appendix 4
AEM QC Maps – Residual, DOI, No Datapoint, TX Height

Appendix 5
AEM Vertical Sections

Appendix 6
Comparison of AEM Models with Lithologic Information

Appendix 7
Magnetic Maps

Appendix 8
SkyTEM Raw Data Report

Appendix 9
TEM Introduction and Theory

ABBREVIATIONS

1VD	First Vertical Derivative
AEM	Airborne Electro-Magnetic
ASL	Above Sea Level
BGL	Below Ground Level
DOI	Depth of Investigation
DEM	Digital Elevation Model
DWR	Department of Water Resources
EM	Electro-Magnetic
Ft	Feet
GAP	The Stanford Groundwater Architecture Project
GERDA	Geophysical Relationship Database
GPS	Global Positioning System
HCM	Hydrogeologic Conceptual Model
HGG	Hydro Geophysics Group – Aarhus University
Hz	Hertz
IGRF	International Geomagnetic Reference Field
KPH	Kilometers Per Hour
LCI	Laterally Constrained Inversion
M	Meter
MPH	Miles Per Hour
MUDP	The Environmental Technology Development and Demonstration Program
NAD83	North American Datum 1983
NIA	Number of turns times current times area of the AEM transmitter system
OHM-M	Ohm Meter
QC	Quality Control
SCI	Spatially Constrained Inversion
SLO	County of San Luis Obispo
TEM	Transient Electro Magnetics
TTEM	Towed TEM
TMI	Total Magnetic Intensity
USCS	Unified Soil Classification System
UTM	Universal Transverse Mercator

1. INTRODUCTION

The project was initiated by acquisition of a few lines of towed TEM (tTEM) surveying along and within the Santa Ynez riverbed with the purpose to evaluate the surface water groundwater interaction in the riverbed. A larger regional airborne electromagnetic (AEM) survey was done in the northern part of the basin with the purpose to map the general geologic and hydrogeologic settings in the area. A location map of the geophysical investigations area is shown in Figure 1.

Figure 1 Outline of the Santa Ynez River Valley basin (blue), AEM survey lines (white) and tTEM survey lines (green).

The two TEM methods as applied provide similar type of data. The tTEM methods cover the depth interval from the surface to approximately 75m (246 ft) compared to the applied AEM method – SkyTEM312 that typically will reach a depth of up to 300m (1000 ft). The footprint of the SkyTEM312 is significantly larger, and the resolution near the surface is not as detailed as for the tTEM method.

1.1 The tTEM Survey

A towed TEM (tTEM) survey was conducted during August 18-19, 2020 in the riverbed of the Santa Ynez River.

Figure 2 TTEM survey lines. The blue lines represents data used for inversion. The red lines represents data removed due to noise from man-made installations.

The objective of the tTEM survey was to provide geophysical results to assist geological interpretations of the geology along the river.

1.2 The AEM Survey

In November 2020, an airborne geophysical survey mapping exercise was carried out using the SkyTEM Survey APS (SkyTEM) airborne time-domain electromagnetic (AEM) system over the Santa Ynez Eastern Management Area of the Santa Ynez River Valley basin in Santa Barbara County, California. The objective of the AEM survey was to provide geophysical results to assist geological interpretations to support data gaps identified in the GSP for the Eastern Management Area.

The AEM survey design, data collection, data processing, and inversion is described as follows:

- The survey design, including flight path definition, selection of the AEM system and regional geologic and hydrogeologic setting.
- The field operation, including an overview of the AEM system used for the acquisition of the electromagnetic data for the Santa Ynez survey area and raw data quality control.
- The data processing of the raw Santa Ynez AEM data to remove noise and related anthropogenic effects or artifacts in the data.
- The application of a non- linear 1D Surface Constrain Inversion.
- Quality control measures during processing and inversion.
- Various types of geophysical maps and sections obtained from the inversion of the AEM data.

The report appendices include presentations of the geophysical results in terms of resistivity maps and cross sections. The report does not include documentation for the calibration and the specific configuration of the AEM system as this information has been described in the acquisition report by SkyTEM (2020) (appendix 8).

Figure 3 Location map of the survey area. Yellow lines show the planned flight paths.

This study area covers the Eastern Management area (EMA) of the Santa Ynez River Valley Groundwater Basin as illustrated in Figure 3.

2. AEM SURVEY DESIGN

2.1 Regional Geologic and Hydrogeologic Settings

The EMA is bounded on the north and east by impermeable rocks of the San Rafael Mountains and to the south by the Santa Ynez Mountains.

The main structural features of the Basin are a pair of the synclines and anticlines, which represent folded formations in the lowland between the Santa Ynez Mountains on the south and the faulted San Rafael Mountains on the north. The San Rafael Mountains to the north of the EMA were uplifted along the Little Pine fault zone, which trends northwest and has a displacement of several thousand feet.

Most of the extraction wells in the groundwater subbasin extract water from the Paso Robles formation. It is a complex formation of folded and faulted Pliocene-Pleistocene unconsolidated non-marine sediments. The sediments defining the Paso Robles formation can be described by a large sequence of layers changing between coarse and fine material. The Paso Robles formation is found at the ground surface in most of the survey area except in the riverbeds where quaternary sediments are found and in certain areas to the south where Paso Robles formation might have been eroded.

2.2 AEM System and System Settings Selection

The AEM system was configured to gain information to the greatest depth possible. Forward modelling studies showed that an AEM system with a peak transmitter moment of 500,000 NIA (number of turns in the transmitter loop, max. transmitter current, area of the transmitter loop) would provide information to a depth of approximately 300m (1000 feet). This is within the main depth interval within the Paso Robles formation where most water wells are screened.

2.3 Flight Line Planning

The overall flight line direction was chosen to be South West to North East, which is perpendicular to the main fault lines and geologic structures within the basin, and therefore would provide the best lateral resolution of the geology. The flight line spacing was selected to be 250 meters (820 ft) for most part of the survey, except the most southern part where the flight line spacing was 500m (1,640 ft). The planned flights lines are illustrated in **Error! Reference source not found.**. The length of the flight lines ranged from 4 to 16 km (2.5 – 10 mi). Two extended flight lines in the center of the survey area connects the main survey area with the area along the Santa Ynez River. To the southwest two lines were flown to map the expected more complex geology west of Solvang to determine the hydraulic connectivity from the north towards south in this area.

Figure 4 The tTEM system being pulled by an ATV.

A significant part of the basin is urban or characterized by vineyards where metal wires supporting the vines are likely to cause interference with the AEM data. Flight lines have been removed or shortened where interference from man-made installations (e.g. crossing vineyards or urban areas) occurred.

3. TTEM FIELD OPERATION

The tTEM survey was carried out by Ahmad-Ali Behroozmand and Emily Cox during August 18-19, 2020. The data collection was performed by towing the tTEM system behind an ATV using a specially designed sled frame with non-metallic parts to avoid potential interference. The equipment was transported to and from the site with a box truck.

The tTEM system went through a detailed test and documentation process at the National Danish Test site. The test results demonstrate that the tTEM system reproduces the reference site

accurately. Detailed information about the TEM methods and the tTEM specifications can be found in a study by Auken et. All (2018).

The tTEM field operation was challenged by the very hot temperatures and limited access to the areas. Some of the survey lines were done outside the riverbed. Many of the planned survey lines were located too close to man-made installations, such as power lines or other metal objects. As a result, those data were contaminated by noise and could not be used in the modelling.

4. AEM FIELD OPERATION

The SkyTEM survey was carried out during November 15-21, 2020. A total of 991.2 line-km of data were acquired, including 9 km (5.6 mi) of repeat lines. The flight line spacing was 250 m with a flight line direction of 34°/214°.

Figure 5 The AEM sensor while being maintained at the local landing site.

The nominal flight speed was in the range of 80-100 kph with an average flight speed of 89.4 kph, depending on the roughness of the terrain and the wind conditions. The average acquisition height was 56.8 m (frame height) with a standard deviation of 16.6 m, but this was strongly dependent on the roughness of the terrain or any obstacles or hazards on the ground. A map showing the flight height for the entire survey is presented in Appendix 4. For most of the survey, the flight height was between 35 and 60 m.

A more detailed description of the survey and SkyTEM system specifications can be found in the survey acquisition report from SkyTEM, Appendix 8.

4.1 The SkyTEM System

The helicopter-borne SkyTEM time-domain electromagnetic system is carried as a sling load beneath the helicopter (Figure 6). The system is designed for hydrogeological, environmental, and mineral investigations. The following section gives a general introduction to the SkyTEM system, while a more comprehensive technical description of the SkyTEM method can be found in a study by Sørensen et al. (2004). A description of the TEM method in general can be found in a study by Nabighian et al. (1991), while a short summary of the method can be found in Appendix 9.

The SkyTEM312 system has a transmitter loop area of 342 m^2 and is made up of a hexagonal frame towed beneath the helicopter. The receiver Z-coil is mounted on the back of the hexagonal frame, approximately 2 m (6.6 ft) above the frame in a near null position relative to the primary field – to obtain close to zero coupling to the transmitted primary field.

The SkyTEM system operates in a dual moment mode, a Low moment (base frequency of 210 Hz, current 6 A) and a High Moment (base frequency of 15 Hz, current 110 A), which are transmitted sequentially. In the Low Moment (LM) mode, a low current, high base frequency and fast switch-off provides early time gates (time windows) for information about the shallower portion of the subsurface. The High Moment (HM) mode, with a higher current and a lower base frequency, provides later time gates for deeper imaging.

Two laser altimeters are placed on the frame, which continuously measure the distance to the ground surface, and two inclinometers measure the roll and pitch of the frame. Power is supplied by a generator placed on the sling cable. The positions of the various devices on the frame are shown in the survey acquisition report by SkyTEM, Appendix 8.

In addition to acquiring electromagnetic data, which provides information about the resistivity structure of the ground, the system also collects magnetic data, which are primarily used for mapping magnetic anomalies, fractures, faults and metallic objects. Auxiliary data is also recorded and includes GPS data for positional accuracy, laser altimeter data and video for a record and review of the ground that is overflown.

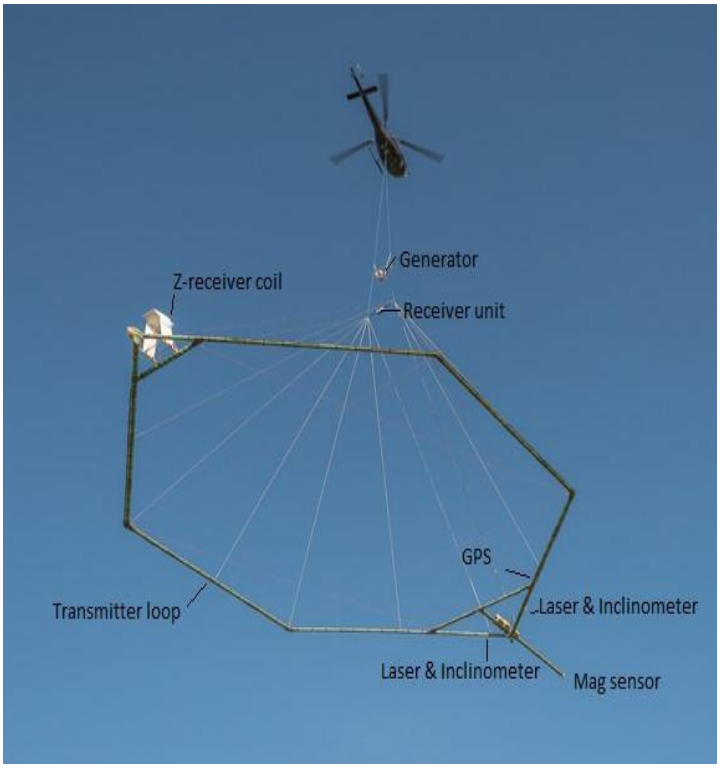

Figure 6 The SkyTEM system. The transmitter frame holds the inclinometers, laser-altimeters, receiver coils and instrumentation.

The SkyTEM system used for Santa Ynez survey collected data with a 210/30 Hz repetition frequency for LM and HM respectively, equivalent to 210/30 decay curves per second. The high number of data points allows for an advanced data processing scheme to achieve the best possible signal-to-noise ratio. The SkyTEM system has been calibrated at the Danish National Reference site. Further details can be found in the SkyTEM acquisition report (Appendix 8).

4.2 Quality Control of SkyTEM Data

Both during and after the acquisition of the SkyTEM data, several measures were taken to ensure that the quality of the acquired data was acceptable. During the flight planning stage, the flight lines were defined in collaboration with the client. This process included determination of flight direction, line spacings and the location of the flight lines. During the initial on-site SkyTEM system set-up phase, high-altitude tests, waveform, configuration settings and null positions were checked in collaboration with SkyTEM to ensure that the configuration and specifications were as agreed upon in the contract.

During the survey, SkyTEM provided daily updates, including a flightpath map of daily production, high altitude test, raw electromagnetic and magnetic data and repeat line data. This allowed for a daily quality control check, which included the following steps:

- Check that acquired data corresponded to planned flight lines and contained no significant, unexplainable deviations.
- Check that transmitter currents are within specifications.
- Check that secondary flight parameters, i.e. flying height and pitch and roll, are within specifications.
- Check the validity of the electromagnetic data, both by inspecting EM response data and by running preliminary inversions.
- Document repeatability (see Section 4.2.2).
- Present preliminary results to the client.

The quality of the data evaluated during the flight operation was found to be acceptable

4.2.1 Weather and General Operational Conditions

As weather can impact the acquisition of EM data, keeping a record of the weather conditions during the survey is useful. During the seven acquisition flights conducted November 15th to 21st, the visibility was good to excellent. Temperatures during acquisition were between 15-28°C (59-82°F) with wind speeds of up to 10 m/s (22 MPH). The weather did not influence the flight operation or quality of the AEM data

4.2.2 Repeat Lines

To demonstrate the repeatability of the SkyTEM system during acquisition, a repeat line was chosen to be flown once per each acquisition flight. This resulted in six repeat lines of approximately 1,400 m length (see Figure 8 for location), two for each day (16th, 20th, 21st). This procedure documented that the AEM system was not affected by drift and caught any issues with the instrumentation during the survey. It also showed that the processing and inversion schemes were consistent.

The data processing of the repeat lines was performed using the same approach as used in the entire survey area, except data potentially influenced by the presence of vineyards were not removed. The inversions of the repeat lines were done by inverting each line data individually, using a laterally constrained inversion (LCI) approach. The inversion results from the repeat lines were compared (as opposed to comparing the raw EM responses). This ensured that

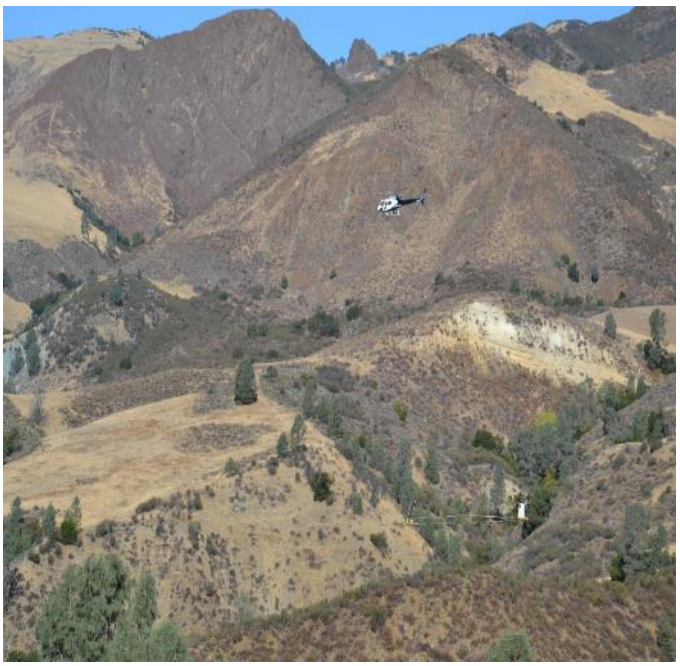

Figure 7 The helicopter flying the AEM system draped the terrain to obtain a nominal flight height of 30-50m above ground.

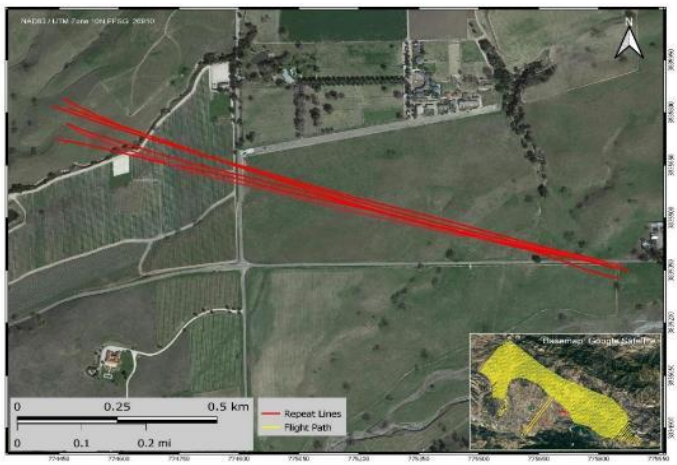

Figure 8 Location map of the six repetitions of the repeat line.

variations in transmitter height, small changes in transmitted current resulting from variations in outdoor temperature and variations in the attitude of the transmitter frame (accounted for in the data inversion) did not affect the comparison.

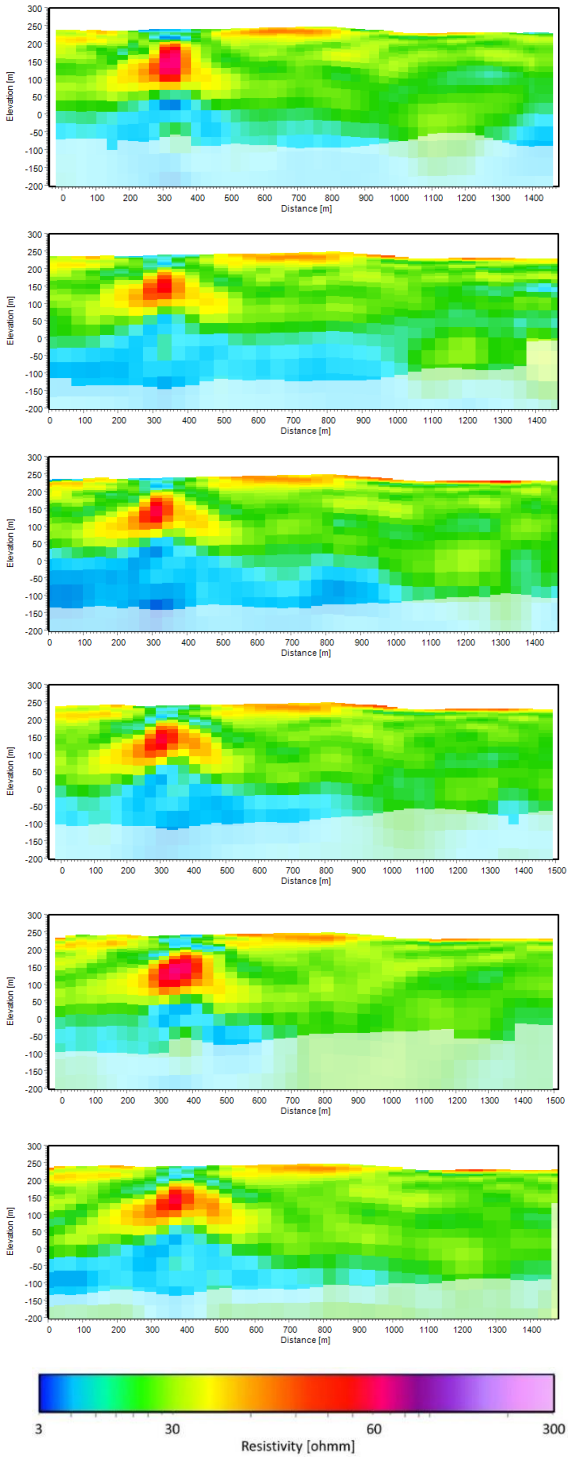

Figure 9 Comparison of the inverted models from the six repeated flights along the repeat line.

The results of the repeated survey lines demonstrate a high repeatability as seen in Figure 9. The comparison furthermore provides a good indication of the level of details that can be obtained within the survey area.

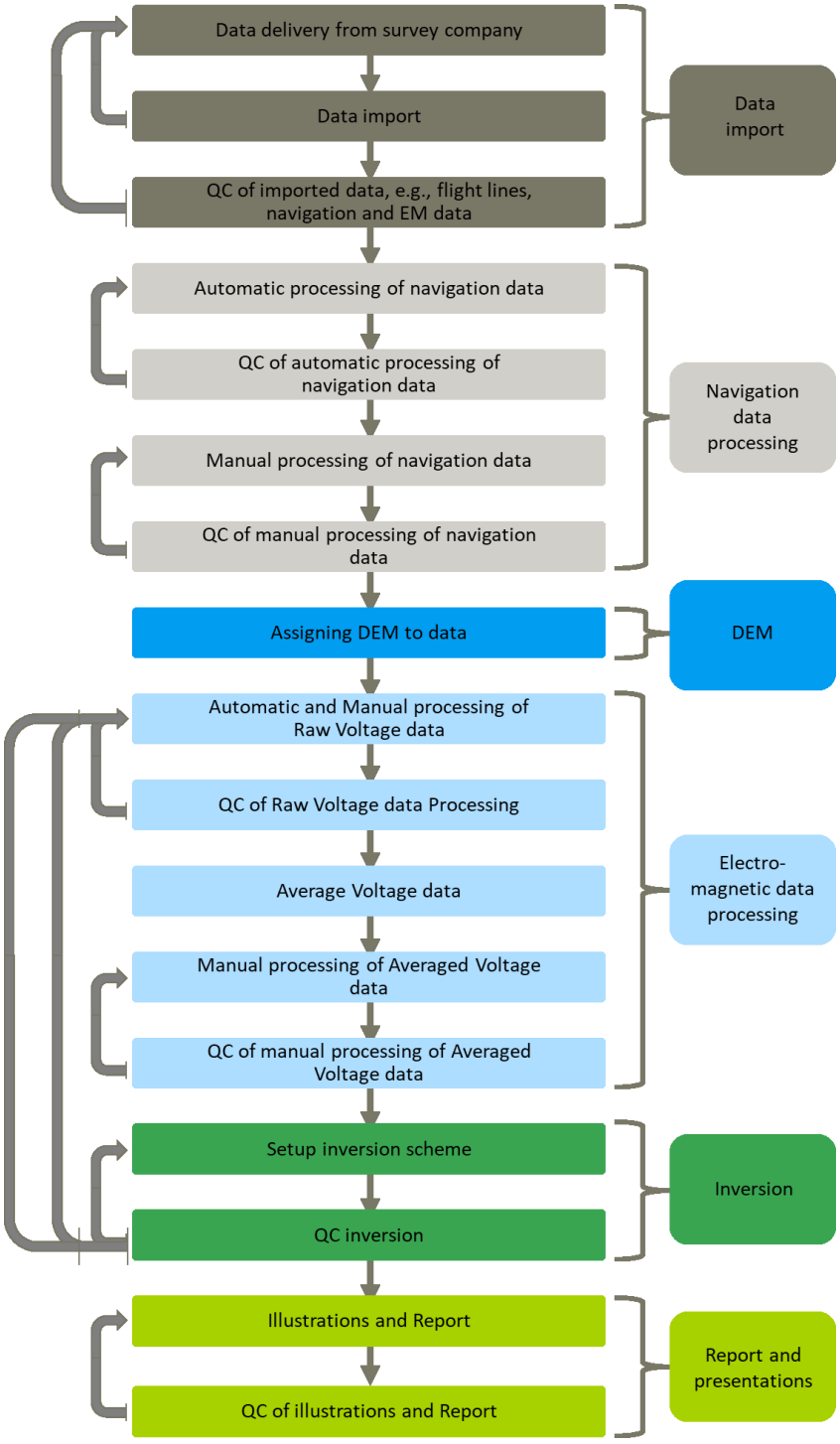

Figure 10 Workflow diagram showing the steps involved in processing and inversion of the SkyTEM data using the Aarhus Workbench software.

5. AEM PROCESSING AND INVERSION

The electromagnetic data were processed to prepare them for inversion. The processing scheme consists of both automatic and manual steps and involves filtering, averaging and removing noisy data. The automatic step requires the user to choose parameters for the filtering and averaging processing routines. The manual step is a step where late time noise and data affected by cultural effects (e.g., overhead powerlines) are assessed according to predefined standards and procedures and removed if needed. The pre-inversion processing is an iterative process as it is often necessary to revisit the data after initial inversion results are visualized.

The inversion scheme employed in Aarhus Workbench uses a full non-linear 1D inversion algorithm with the option of applying lateral constraints along and across flight lines, to allow the migration of information between neighboring soundings. Inversion of electromagnetic data is the process of transforming the measured EM responses to a resistivity-depth structure of the subsurface. The inversion algorithm requires user input, such as model discretization, starting resistivities, and horizontal and vertical constraints. A resistivity-depth model was obtained for each individual sounding along a flight line. These models can be stitched together to form 2D sections or combined into 3D grids to provide spatial information of the resistivity structure of the subsurface.

The processing and inversion of the SkyTEM data were completed using the Aarhus Workbench software package. The workbench is a well- documented and technically sound software package developed for processing and inversion of electromagnetic and geoelectrical data. The steps involved in the processing and inversion of data will be described in detail in the following sections and an overview of the workflow is shown in Figure 10.

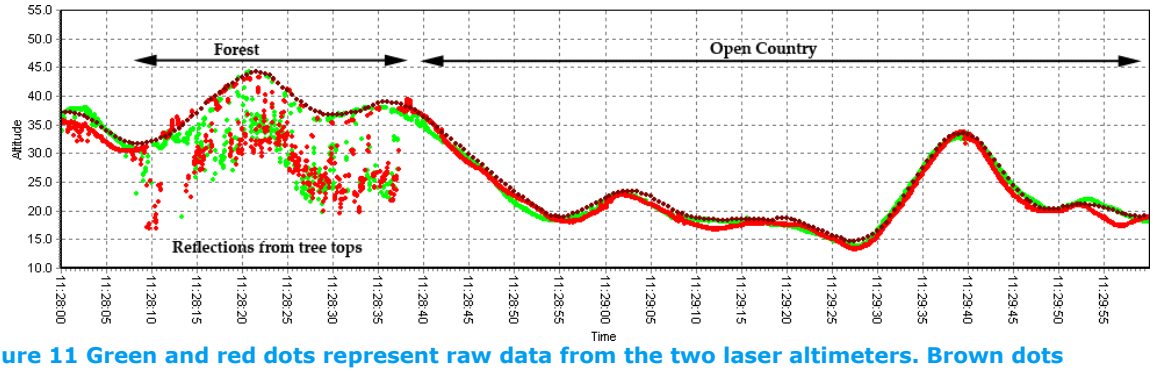

Figure 11 Green and red dots represent raw data from the two laser altimeters. Brown dots represent the height after filtering the data. The time window covers approximately 2 km of data.

5.1 Data Import

Data were imported to the processing and inversion software. There were no problems importing the data.

5.2 Navigation Data Processing

The processing procedure involved processing both auxiliary data and electromagnetic data. The workflow and order of the processing steps are seen in Figure 10. Processing of Auxiliary data consisted of an automatic filtering of the GPS, roll and pitch and transmitter height data. Furthermore, processing of the transmitter height data involved a manual step to ensure that outliers or spikes in the data were appropriately removed or filtered.

5.3 GPS Positions

Two GPS receivers located on the transmitter frame measured the position of the frame during data acquisition. The GPS data, from the GPS base station and GPS receivers mounted on the system, were postprocessed by SkyTEM to obtain differentially corrected positions. An automatic processing of the GPS positions was applied in the Aarhus Workbench. As the GPS receivers were mounted in the front of the system, the coordinates were moved to reflect the center of the system. The processed GPS positions were extracted at every 0.5 second.

5.3.1 Pitch and Roll

During acquisition flights, the altitude of the transmitter frame was measured. The roll and pitch of the frame were subsequently used to correct the height and electromagnetic responses for their deviation from horizontal. It was presumed that the frame was rigid so that the roll and pitch of the transmitter loop and receiver Z-coils were identical (see Appendix 8 for further details of the SkyTEM system). The automatic processing of the roll and pitch data was done using standard parameters. The roll and pitch data were then checked and accepted. Maximum angles of 10 degrees were maintained throughout the entire survey.

5.3.2 Transmitter Height Data

The distance between the transmitter loop and the ground was measured with two independent laser altimeters. The height of the transmitter frame was used as an input to the inversion of the EM responses. This parameter can impact the inversion results if it is not measured or modelled correctly.

The processing of the transmitter height (from the ground surface) involved both an automatic filtering and averaging step and a manual step involving inspection and correction of data points. The manual step was required to remove outliers and to correct the height in areas where the laser altimeters were reflected by things other than the ground surface resulting in a wrong transmitter height. An example of this is reflection from treetops (canopy effect), which resulted in an apparent lower height than if it would reflect from the ground surface (Figure 11 shows an example of height data). A figure of the corrected transmitter height is shown in Appendix 4.

Only a few manual edits were applied since dense tree coverage within the survey area is very limited.

5.3.3 Digital Elevation Model

To relate the inverted resistivity-depth models to the topography of the landscape, a digital elevation model (DEM) of the area was required. For this survey, the USGS 1/3 arc-second DEM of the study area was used during the processing and inversion of the SkyTEM data. The DEM was added to the data after processing of the navigation data (see Figure 10 for the workflow).

5.3.4 Processing Electromagnetic Data

The automatic processing of the electromagnetic data included averaging and applying a trapezoidal filter, as well as filters to automatically remove data influenced by couplings and late time noise. The manual processing involved a check of the automatically filtered data and additional noise removal as needed.

It is common to find that data acquired near powerlines, roads, railroads, and other manmade installations are heavily affected by these noise sources as the electromagnetic responses couple to them. To avoid artefacts generated by the coupled data in the inversion results, the affected data points were removed before the inversion.

During flight operations, a digital camera with geographical coordinates was employed. The video was reviewed, and locations were noted where powerlines, railroads, irrigation pipes and other potential noise sources were present. The information was saved in a GIS layer and used to identify coupled (noisy) data while processing the AEM data.

To maximize the lateral resolution, no further stacking (averaging) of the raw data was applied, resulting in a sounding for each 1.3 s (approximately 32 m or 105 ft, depending on flight speed). The data uncertainty was calculated from the raw data stack, with an additional 3% uniform data uncertainty added.

A diagram of the SkyTEM data processing is shown in Figure 10. First, the coupled data parts were removed from the raw data. Then data were stacked into soundings, and an averaging trapezoidal filter was applied. Finally, the late-time part of the sounding curves below the background noise level was excluded. The final manual processing ensured that adequate noise and coupled data were removed before inversion of the data. The automatic filter settings can be found in Appendix 1.

5.4 Quality Control of the Data Processing

The data were first verified in Aarhus Workbench using a geometry setup file (.GEX file). The system information found in the geometry file included waveform definitions and time gates that, if not specified correctly, would impact the data modelling. The information in the geometry setup file was checked against the system specifications stated in the acquisitions report provided by SkyTEM and it was confirmed that all relevant data were delivered by SkyTEM and imported correctly.

Several quality control (QC) steps are followed throughout the data processing stages (see workflow diagram in Figure 10) and form a logical part of the iterative processing workflow. The manual processing step included a visual inspection of the data after the automatic processing to assess if the manual processing was sufficient, while making necessary adjustments (e.g. the late time noise or data affected by couplings) found either in the averaged or raw EM responses.

Preliminary inversions were run after the data processing steps to ensure that the data processing was adequate and that artifacts from the unprocessed noise in the data were not introduced to the inverted models. The preliminary inversions were also used to test and adjust inversion settings.

5.5 Inversion

The Aarhus Workbench uses the 1D full non-linear inversion algorithm AarhusInv (Auken et al., 2015). The AarhusInv inversion algorithm counts for the Low and High moment SkyTEM data and the transmitter loop height simultaneously. In addition to the measured EM data, this type of inversion algorithm needed a model discretization and parameter values for vertical constraints to define how much resistivity of each layer can vary with respect to the neighboring layers. Another option was to constrain all resistivity models laterally along the flight lines or spatially across the flight lines to allow for the migration of information from one flight model to another (see section 5.3).

5.5.1 Spatially Constrained Inversion

The Spatially Constrained Inversion (SCI) was used for the inversion of the Santa Ynez data (Viezzoli et al, 2008). The specific settings of the SCI inversion can be found in Appendix 1. The inversion scheme was based on a 1D forward solution where spatial constraints across flight lines

were applied. Constraints were built using Delaunay triangulation, and the inversion approach accounts for all model parameters, electromagnetic data, and constraints.

Benefits of using the SCI method as opposed to other inversion schemes (Single Site or Laterally Constrained Inversion) include:

- Suppression of elongated structures, a common feature when using Laterally Constrained Inversion where lateral constraints are only applied to neighboring models along flight lines, not between models on neighboring flight lines.
- A better resolution of otherwise poorly resolved parameters, e.g. relatively thin layers and layers with high resistivity like sandy aquifers.
- A smooth quasi-3D model representing 3D geologic variation.
- Transfer of information across flight lines.

5.5.2 Smooth Layer Inversion Setup

A 30-layer smooth model was used for the inversion of the Santa Ynez SkyTEM data. In this type of inversion, the resistivity of each layer varies while layer thicknesses remain fixed. Typically, layer thickness increases with depth as the sensitivity of the method decreases with depth. To stabilize the inversion, vertical constraints are typically applied between layer resistivities, which enforces a smooth transition from one layer to the next. This type of inversion produces smoothly varying resistivity-depth models, which can smear out specific layer boundaries, compared to a model with few layers.

The first layer thickness was chosen to be 1 m with logarithmically increasing thicknesses to a depth of 700 m, which was the depth of the last layer boundary. The resistivities of the starting model for the inversion was chosen automatically by Aarhus Workbench. More information about the inversion settings can be found in Appendix 1.

5.5.3 Depth of Investigation

The resistivity-depth models derived from the inversion of AEM data can be misleading if no information is given about the depth of investigation (DOI) of the AEM system. The DOI gives an indication of a depth to which a resistivity-depth model can be considered reliable. Values at or around the depth of investigation should therefore be interpreted with caution.

The depth of investigation is a complex measure, and the method used here was based on the cumulative sensitivity of the actual model output from the inversion, the actual full system response and geometry, the data noise and the number of data points (Christiansen et al., 2012).

Typically, a depth of investigation of 150-400 m (492-1,312 ft) can be achieved, but this is strongly dependent on the above-mentioned parameters. In general terms, a decrease in the subsurface resistivity results in a reduced DOI, and an increase in the subsurface resistivity results in a greater DOI (a map showing the DOI for the survey area is found in Appendix 4).

5.5.4 Quality Control of Inversions

An important step in the inversion of the dataset was setting up the inversion model and choosing inversion parameters, including choosing thicknesses and number of layers, as well as inversion constraints. These parameters impact the inversion results.

When the inversion model was chosen, consideration was given to the known geology of the area (e.g., whether the geology is expected to be horizontally layered or containing vertical or complex geologic structures) and a model setup which best represented the geology of the chosen area. After the initial inversion results were assessed, the inversion parameters were evaluated and

adjusted. Systematic discrepancies between the measured and the modelled responses were checked. These discrepancies can be caused by the choice of inversion parameters, such as thicknesses and vertical constraints.

The data residual, or data fit, was used to evaluate the inversion results. A data residual of 1.0 or below corresponds to data being fitted within the uncertainties assigned to the data. A high data residual indicates that the inversion scheme was unable to find an acceptable model that can fit the data. The residual values for this survey were generally below 1.0. For some areas, the data fit was slightly higher but still within an acceptable range.

Another useful measure in assessing the inversion results is to look at the number of data points. This gives an indication of how many data points are left after data processing, for example, after removal of late-time noise and coupling. The more data points, the better the signal to noise ratio and the more reliable the inverted models, particularly at depth. Typically, a lower number of data points are noted in resistive areas and in areas with a high acquisition height. Appendix 4 shows the number of data points after processing, which were satisfactory and above normal.

6. PRESENTATION OF RESULTS

The inversion of the geophysical data produces a large number of one-dimensional (1D) vertical models tied together, creating a 3D resistivity image of the subsurface. The resistivities can be stitched together to form 2D vertical sections or cut into depth or elevation slices to show the spatial distribution of mean resistivities at different depth or elevation intervals. The modelled resistivities can represent different lithologies used for geologic interpretations.

6.1 Resistivity Color Scale

An indication of the resistivities of different lithologies was needed to relate the inverted resistivities to lithologies and eventually make geologic interpretations from the inversion results. Translating resistivities to lithology was based on a general correlation between resistivity and different types of sediments and varied between locations. Figure 12 shows a general correlation between resistivity and lithologies. The water quality within the vadose zone/aquifer can change the resistivity due to more saline water having a lower resistivity. Therefore, correlation with additional data sources (primarily information from boreholes) and general geologic knowledge were crucial to obtain the most accurate description of the subsurface.

For the Santa Ynez EMA survey area, a resistivity color scalebar with resistivities ranging from 3-300 ohm-m was used to represent the resistivity variations seen in both the AEM data and tTEM data across the area. The scale bar is shown in Figure 12.

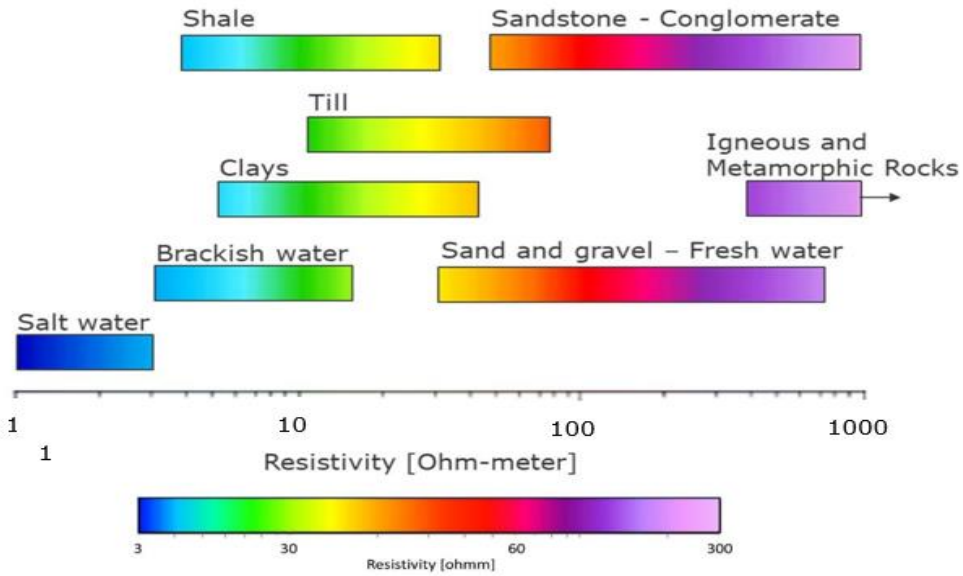

Figure 12 (Top) General correlation between resistivity and type of sediments, (Bottom) the resistivity color scale used in this study for presentation of the AEM results.

6.2 AEM Mean Resistivity Maps

Resistivity-depth (or elevation) maps are a way to spatially visualize the variation in resistivity at different depths across the survey area. Mean resistivity elevation slices were generated from the multi-layer spatially constrained inversion in 20 m (60 ft) intervals from 400 m above sea level (asl) to 0 m asl as presented in Appendix 3. Only inversion results that are above the DOI are shown on the resistivity maps.

The mean resistivities are calculated as the horizontal resistivity (see Appendix 8 for the calculation of the mean resistivities) and are gridded using kriging (gridding method), with an exponential variogram, node spacing 50 m and search radius of 600 m.

The mean resistivity maps show the varying resistivity in the area reflecting the varying geology as described in Section 6.1.

6.3 Resistivity-depth Sections

Vertical resistivity-depth sections based on the smooth and sharp inversion models have been generated for the tTEM profiles and for the AEM lines, respectively.

6.3.1 tTEM Resistivity-depth Sections

The following figures present vertical model sections illustrating resistivity models at different locations and directions (along tTEM survey paths) within the study sites. Detailed structural variations are observed along each section. The data were inverted using the laterally constrained inversion (LCI) approach, which applies lateral constrains between the neighboring models along the paths. The tTEM residuals were low along all surveyed lines that indicates good data fit (see Section 6.4).

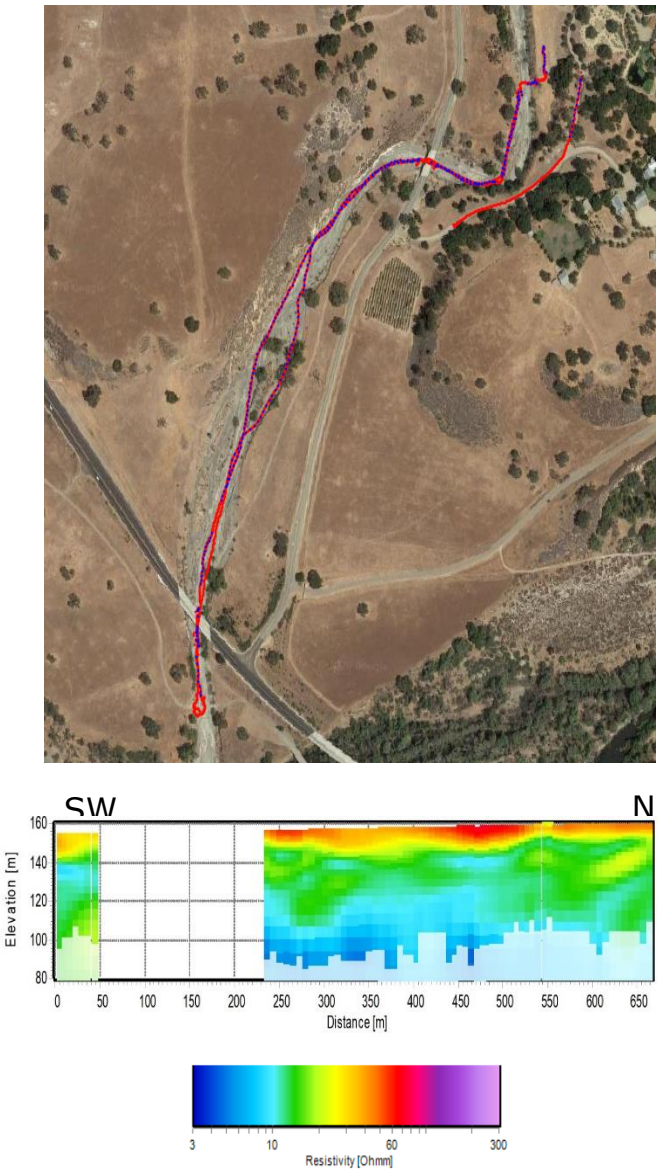

Figure 13 A tTEM vertical section along Santa Aqueda creek.

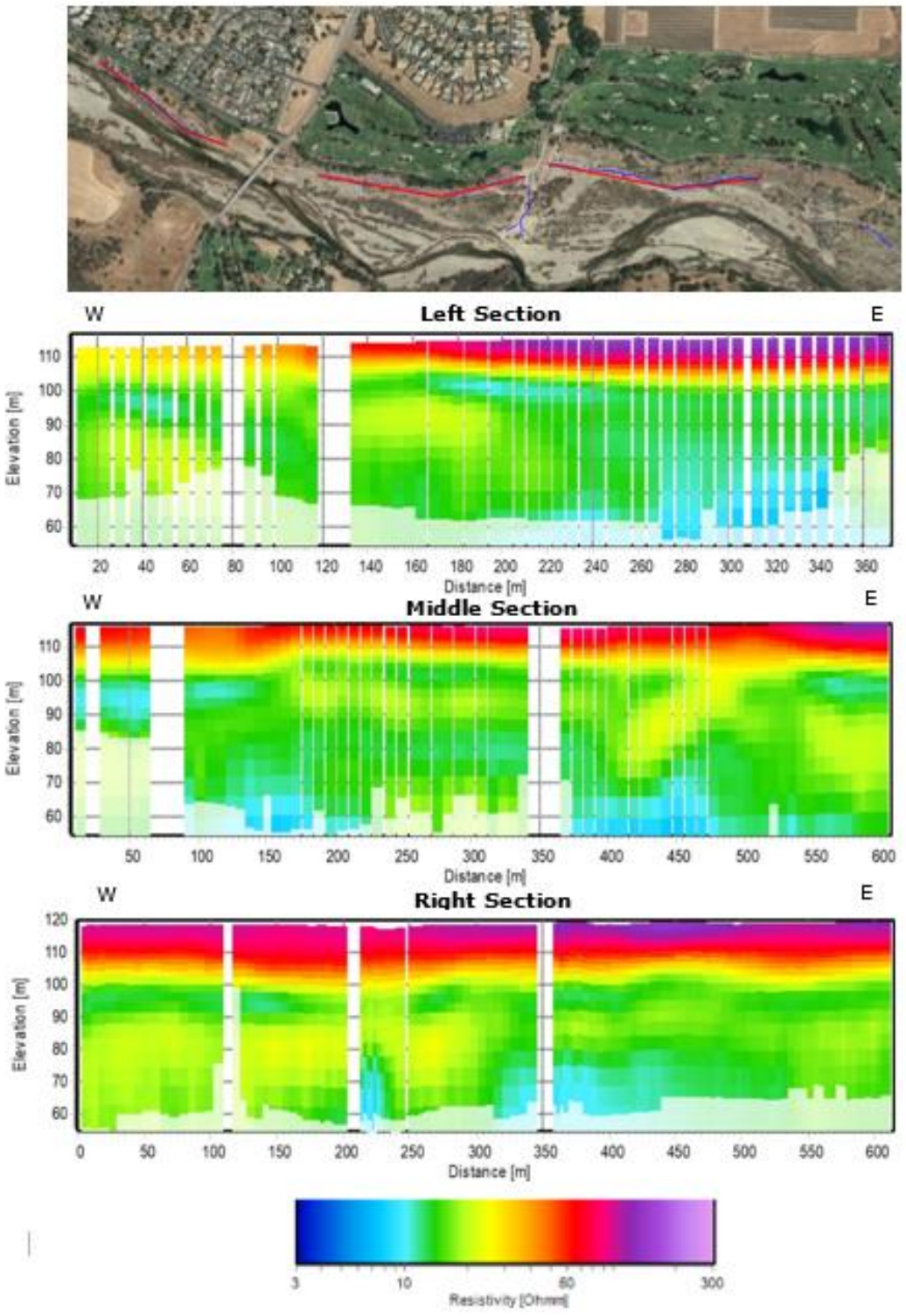

Figure 14 tTEM vertical sections at Alamo Pintado.

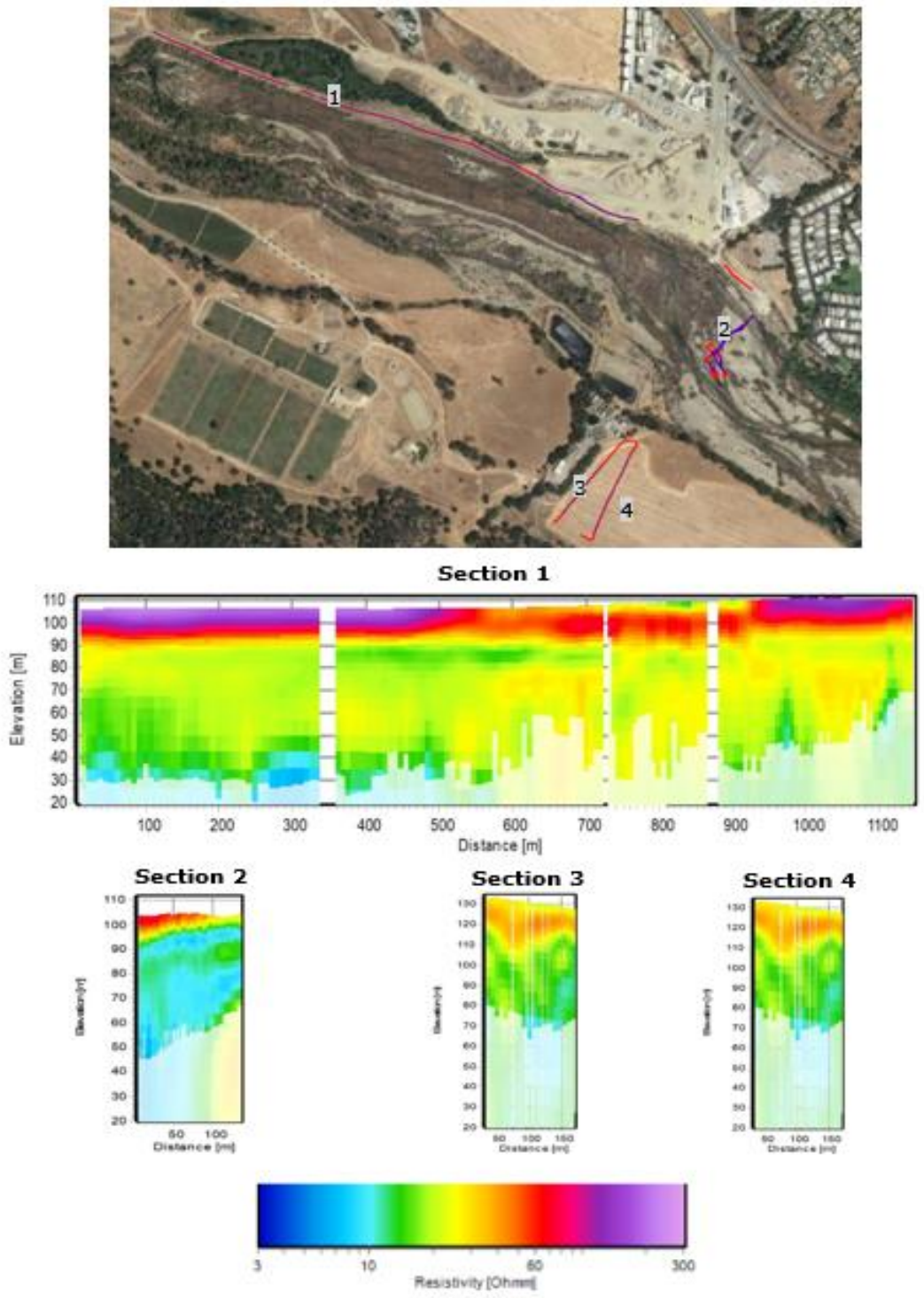

Figure 15 tTEM vertical sections at Adobe Canyon.

The tTEM depth of investigation (DOI) extends to > 75 m below the ground surface (bgs), with smaller DOIs observed at Santa Aqueda creek and larger DOIs observed at Adobe Canyon. The DOI depends on the geologic settings at each site and the data quality determined by the actual ambient noise during the survey, among other factors.

Some of the general observations within different depth intervals at different sites are described below. The observations are obtained based on the resistivity results and assuming that groundwater is of high quality.

- Santa Aqueda Creek: The top 10-15 m bgs consist of high resistivity sediments, indicating coarse materials. Resistivity values in this layer are generally higher towards northeast. Below this layer, a low resistivity layer indicates finer materials. This layer is inhomogeneous with generally lower values in the middle part of the section.
- Zanja De Cota: At this site, the data were dominated by noise due to the presence of metal fence on both sides of the road, overhead powerline and powered cables. The data at this site were found unusable.
- Alamo Pintado: A top high resistivity layer with thickness of up to 20 m is found at this site except for the first 100 m on the left where resistivities are lower. The underlying layer has generally lower resistivities though it is heterogeneous with presence of medium resistivity units across the site, for example the tipped medium resistivity unit shown on the middle section in Figure 14 (distances 400-500 m).
- Adobe Canyon: Section 1 in Figure 15 shows results from the data acquired on the levee. The top layer is resistive for most of the section except for interval 700-900 m where it is capped by low resistivity materials. Below this layer, resistivities are low for the first half of the section, while higher (medium resistivity) values observed to the east. Section 2 crosses the river. A relatively thin high resistivity layer is seen on the top section. The underlying layer has very low resistivities and extend to the depth of investigation. Sections 3 and 4 show similar results with a top medium resistivity layer (~ 20 m thick) followed by a low resistivity unit.

6.3.2 AEM Resistivity-depth Sections

Resistivity-depth sections, based on the sharp SCI models, were generated along each flight line (presented in Appendix 5) and show the resistivity variability in the top 300 m (~1,000 ft). Along the sections the depth of investigation (DOI) has been calculated. Below this depth the colors faded to reflect that the obtained models are more uncertain. The sections are presented in the same horizontal and vertical scale. The two long lines (L106400 and L106600) are presented with focus on the northern area and as sections covering the entire flight lines by the end of the appendix 5.

Each section is presented on a single page as four panels.

- The first panel is a map showing the location of the flight line, the entire section including areas outside the survey line, faults and geologic structures, and location of boreholes.
- The second panel shows a geologic map replacing the Google orthophoto.
- The third panel shows the AEM model section with the terrain model.
- The fourth panel shows the same as panel three and information from nearby boreholes and the existing HCM.

6.4 Data Fit

The data fit or residual is a way to assess if the forward response of the resistivity model obtained from the inversion of the SkyTEM data fit the data within their standard deviations. If the residual was high (much larger than 1.0) meaning the data fit was poor, the forward response from the model would not match the measured response well. Poor data fit might be seen in areas with a lot of 3D structures or in areas with a high noise level (see also section 5.5.4). For the most part, the residual values were low (<= 1.0) meaning the data fit was good overall.

6.5 Magnetic Data

As described in section 4.1, the SkyTEM system also collects magnetic data during acquisition flights. A total magnetic field sensor, located on a boom on the front of the AEM transmitter frame

(see Figure 6), recorded the background magnetic response during the survey. The Total Magnetic Intensity (TMI) and the First Vertical Derivative (1VD) grids are products of the processed magnetic data prepared by SkyTEM (SkyTEM, 2020). The TMI represents the deeper structures, whereas, the 1VD map represents the shallower structures (Appendix 7). The residual magnetic Total Field intensity data for the survey area after correcting for diurnal drift and removing the International Geomagnetic Reference Field (IGRF). The magnetic data are primarily used for mapping magnetic anomalies, fractures, faults and metallic objects.

7. INTERPRETATIONS

7.1 Regional Geologic Setting and Major Hydrostratigraphic Units

The Santa Ynez River groundwater basin is a complexly folded and faulted structural depression located at the southernmost extension of the Coast Ranges, between the San Rafael Mountains to the northeast and the Santa Ynez Mountains to the south which form the western part of the Transverse Ranges. The Santa Ynez River groundwater and rocks in the surrounding uplands record multiple phases of Miocene and younger tectonism related to; a clockwise rotation of the western Transverse Ranges; the transition of the Pacific-North American plate margin from a transtensional to transpressional boundary, and the resulting slip on major faults west of the San Andreas Fault with associated folding of basin sediments (Sweetkind et al. 2021). Geologic indicators are consistent with reverse displacement with a small dextral component (Cannon, 2013).

The Little Pine Fault which forms the northeast basin boundary is mapped at the surface as a northeast dipping fault thrusting the Franciscan Complex over the Pliocene to Pleistocene age Paso Robles Formation (Dibblee 1993b). The Garey fault is mostly hidden, covered by alluvium and is interpreted from limited subsurface data as a steeply northeast-dipping reverse fault cutting units as young as Paso Robles Formation (Hall, 1981, 1982). A series of northwest striking faults that bounds the western edge of the Zaca oilfield is referred to as the Oceano-Zaca fault and is based on the interpretation of seismic-reflection data (Sweetkind et al. 2021). The Baseline fault is mapped as a reverse fault with an upthrown block to the south (Sweetkind et al., 2021), and has an offset of about 30 m (1 mm/yr. slip rate) and a regional uplift rate of between 1.2 and 1.8 mm/yr. based on work by the California State University Long Beach (CSULB online). The Santa Ynez River fault is concealed and generally lies beneath the Santa Ynez River. Subsurface data suggest dips to the south and has a south-up, north-verging, post-Miocene slip (Sweetkind et al. 2021).

The Santa Ynez River groundwater basin lies within the greater Santa Maria stratigraphic basin, a regional-scale syncline lying between the San Rafael and Santa Ynez Mountains. The basin contains a thick Neogene sedimentary sequence that records Miocene basin subsidence and the development of the transform plate margin. This was followed by gradual shoaling and emergence in the late Miocene to early Pliocene including deposition of the Monterey, Careaga Sand and lower Paso Robles Formations. Transition to compressional tectonics associated with Neogene rotation of the Transverse Ranges ensued on the southern margin of the basin with continued deposition of the Paso Robles Formation. Compression resulted in north-vergent reverse faults and folding of Miocene and Pliocene sediments and formed the anticlinal traps for much of the petroleum formed in the Santa Maria stratigraphic basin. The associated uplift formed the landscape observed today, with the uplands generally underlain by anticlines, and low-lying valleys generally underlain by synclines (Sweetkind et al., 2021).

Major hydrostratigraphic units in the Santa Ynez River groundwater basin from bottom to top include the Miocene Monterey Formation, Pliocene Careaga Sand, Plio-Pleistocene Paso Robles

Formation and Quaternary alluvial deposits. The Monterey Formation is typically considered a low permeability 'bottom' to the groundwater producing strata, although fractures can typically produce enough water to support domestic demands. The Careaga Sand is very fine grained and has been considered problematic, as wells can end up pumping sand, and production while relatively low, can supply some of the demand of adequate water quality. The Paso Robles Formation is the main production aquifer within the Santa Ynez River groundwater basin and provides ample water to meet demands. The surficial alluvial aquifers probably provide the highest production rates but tend to be reactively thin and limited in aerial extent. For more specific information on aquifer hydraulic conductivities, transmissivities and well yields, refer to the draft Santa Ynez River groundwater basin Groundwater Sustainability Plan (GSP).

There is insufficient data to understand and predict how the local basin hydrogeologic structure (faults and folds) may affect groundwater flow. Faults can affect water flow and well production because groundwater movement may be inhibited or preferentially increased across or within faults and fault zones. Faulting can break even very strong rocks, producing fracture zones that tend to increase permeability, and may provide preferential paths for groundwater flow. Conversely, some faults can form groundwater barriers, if the faulting grinds the broken rock into fine-grained fault gouge with low permeability, or where chemical weathering and cementation over time have reduced permeability. The hydraulic characteristics of materials in a fault zone, and the width of the zone, can vary considerably so that a fault may be a barrier along part of its length but elsewhere allow or even enhance groundwater flow across it. Faults and folds also may displace rocks or sediments so that geologic units with very different hydraulic properties are moved next to each other, reducing or constricting flow.

7.2 Resistivities compared to borehole information

Several drillholes are present in the survey area and form the base for the existing Leapfrog model previously generated by GSI. This model generally outlines the major formation boundaries found within the survey area, and the existing model has also formed the base for further interpretation.

Fourteen drillholes were sought out as having a lithological description of high quality and were used as a verification of the AEM modelling results. Appendix 6 shows the fourteen boreholes and their nearest AEM sounding. The boreholes and corresponding AEM models highlight that sediments found within the survey area contain a range of different resistivities, but there may be a bit of an overlap in terms of resistivity ranges for the different sediments, which can make it hard to distinguish between the sediments and formations based on the resistivity intervals alone.

Within the AEM survey area, a total of 14 boreholes were selected, and the accompanying well completion reports (WCRs) have been digitized. The coordinates for the selected boreholes are listed in Table 1. The selection of boreholes is based on an evaluation of the quality of the lithological descriptions. In Appendix 6, the lithology for all the boreholes is listed. The lithology has been transcripted as stated in the WCR and then interpreted based on the Unified Soil Classification System (USCS) and a very simple division in coarse and fines.

Saturated and unsaturated sediments will vary in resistivity. To support the interpretation the water level was initially visualized on the vertical sections. As the number of boreholes with water level measurements and information about the screening intervals are very sparse, it can be questioned if the grid-surface is useful across the basin. We could not readily identify a correlation between the resistivities and the water levels, and as the geology represented by the AEM models is rather complex, the water levels were omitted from all the presentations.

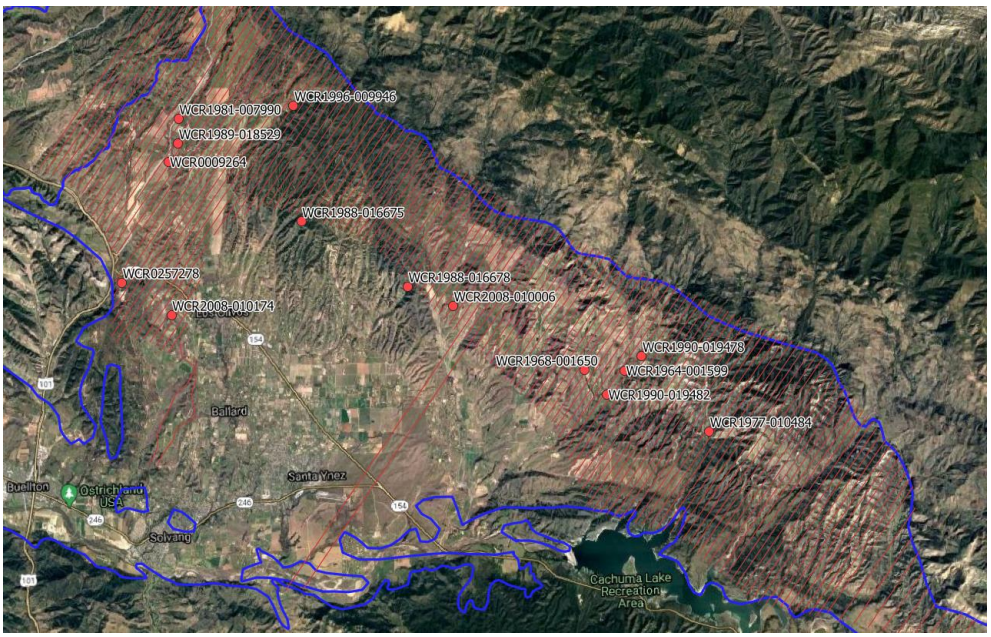

Figure 16 Location of boreholes that have been digitized.

Table 1 List of boreholes that have been digitized.

Borehole ID	Topography (ft)	Easting (m)	Northing (m)	Map datum
WCR0009264	966	762452	3845345	NAD83 UTM Zone 10N
WCR0257278	843	760782	3841039	NAD83 UTM Zone 10N
WCR1964-001599	1020	778783	3837891	NAD83 UTM Zone 10N
WCR1977-010484	924	781802	3835720	NAD83 UTM Zone 10N
WCR1981-007990	1023	762802	3846892	NAD83 UTM Zone 10N
WCR1988-016675	1190	767205	3843215	NAD83 UTM Zone 10N
WCR1988-016678	1074	771012	3840900	NAD83 UTM Zone 10N
WCR1989-018529	1009	762791	3846009	NAD83 UTM Zone 10N
WCR1990-019374	1095	763477	3847637	NAD83 UTM Zone 10N
WCR1990-019478	1054	779387	3838410	NAD83 UTM Zone 10N
WCR1990-019482	951	778151	3837033	NAD83 UTM Zone 10N
WCR1996-009946	1193	766922	3847366	NAD83 UTM Zone 10N
WCR2008-010006	1109	772631	3840211	NAD83 UTM Zone 10N
WCR2008-010174	1048	762553	3839878	NAD83 UTM Zone 10N

7.2.1 Interpretation of Outcropping Formations West of Los Olivos

In the area west of the city of Los Olivos and east of the La Purisima Hills, the AEM sections reach an area where the Careaga sand is observed at surface (outcropping), see Figure 17. This is an important observation as it provides evidence that the Careaga sand can be correlated with the AEM model layers with higher resistivities.

The Paso Robles formation follows on top of the Careaga sand. The Paso Robles formation is interpreted as being non-marine though it is possible that the deepest parts of the Paso Robles formation are marine sediments. On the AEM sections the layers directly above the Careaga sand

have low resistivities which are interpreted as more fine-grained sediments. It is noted that the resistivity within the Paso Robles formation seems to vary, corresponding to varying layers of fine and more coarse material. It is also worth noting that that the varying layers seen in the AEM models can reflect that a more complex sequence of folded and faulted layers.

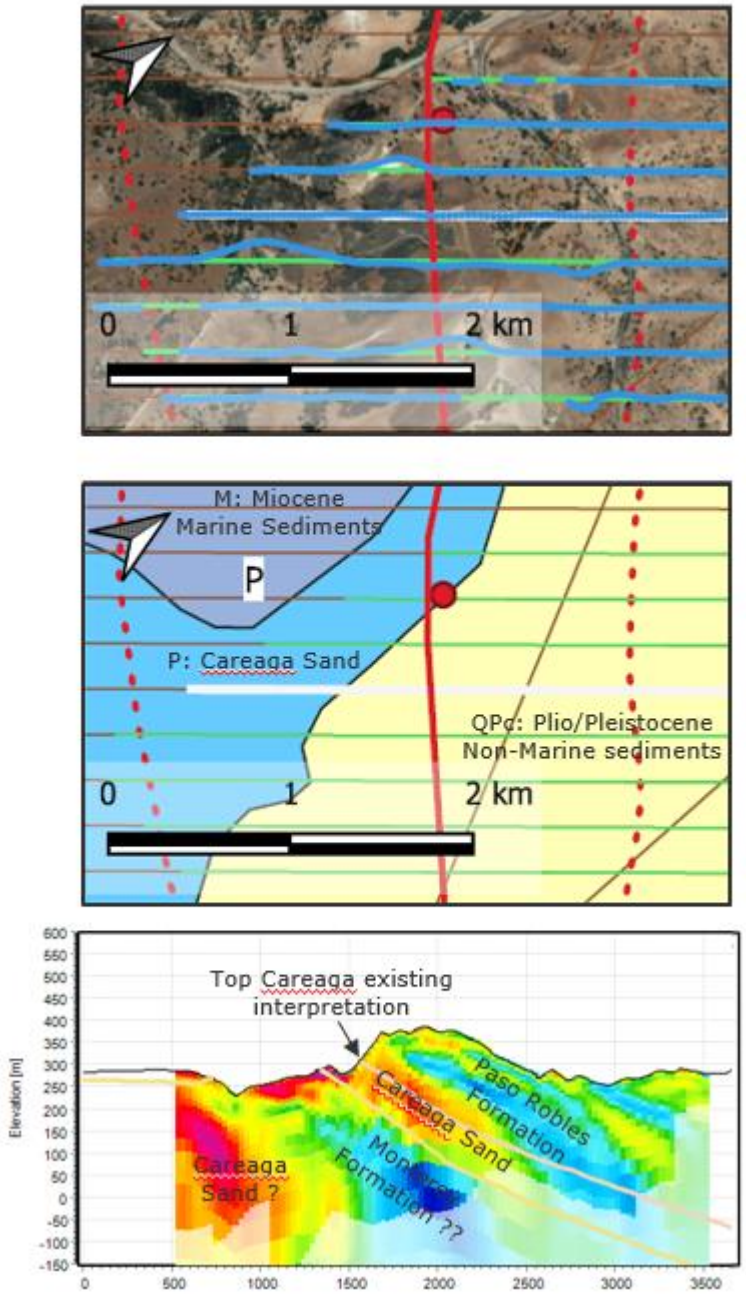

Figure 17 Interpretation of AEM survey line - La Purisima Hills.

7.3 Interpretation with Focus on Specific Geographical Areas

In this section, a combined interpretation of the geophysical models with existing interpretations and borehole information is discussed. It is the intent that the interpretation of the selected sections can be used as a recipe for how the remaining sections may be interpreted. The AEM sections show the layers from the existing hydrogeological conceptual model (HCM).

Starting from northwest the vertical sections for line L100400, L101600 and L102000 (see figure 18) are presented on Figure 19. On top of the sections a simple interpretation of faults, synclines, anticlines and of the geologic formations are made.

On section L100400 the Zaca Anticline core is composed of the Careaga Sand juxtaposed on both sides by the Paso Robles Formation. This structure is in agreement with previous knowledge from the literature – the new finding is the Careaga Sand at the core. Sweetkind et al. 2021 have mapped the Oceana-Zaca fault on the west side of the Careaga Sand body.

On section L101600 the Careaga Sand forms the major axis of an anticline on the left and has been uplifted relative the adjacent Paso Robles Formation on the right which forms a synclinal with the lower Paso Robles daylighting on the left of the upper. The WCR for borehole WCR 1989-018529 has more than 100m white sand which is interpreted to be Careaga Sand.

On section L102000 from right to left, there appears to be a Paso Robles syncline adjacent to an anticline where Careaga Sand underlies the lower Paso Robles formation, continuing left more anticlinal undulations causing land surface highs with a moving into another Paso Robles synclinal structure further to the left and Baseline thrust fault.

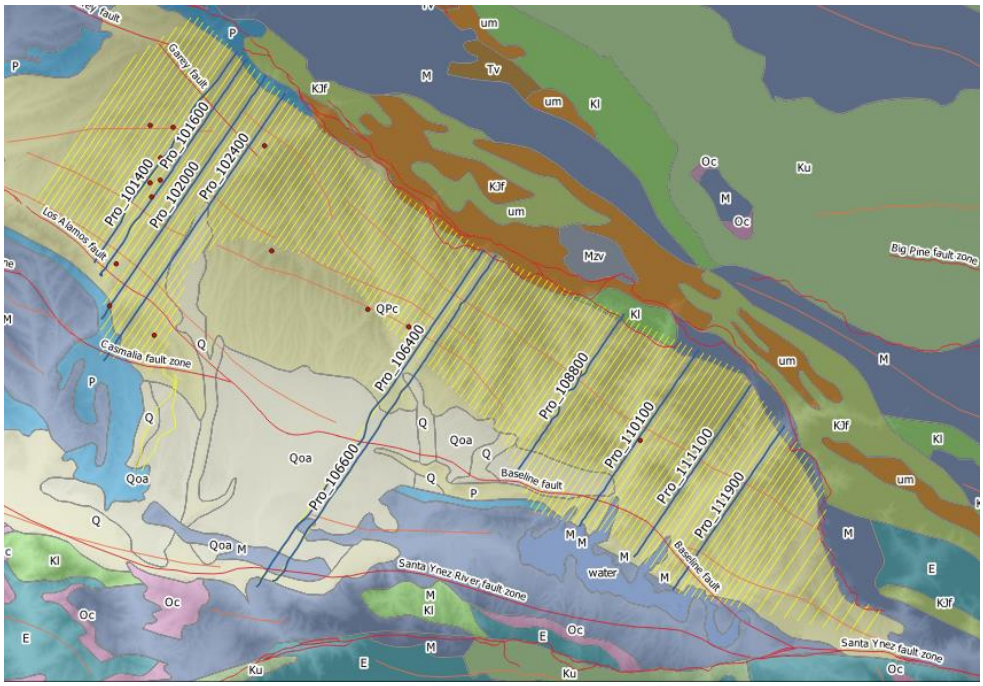

Figure 18 Selected lines for interpretation.

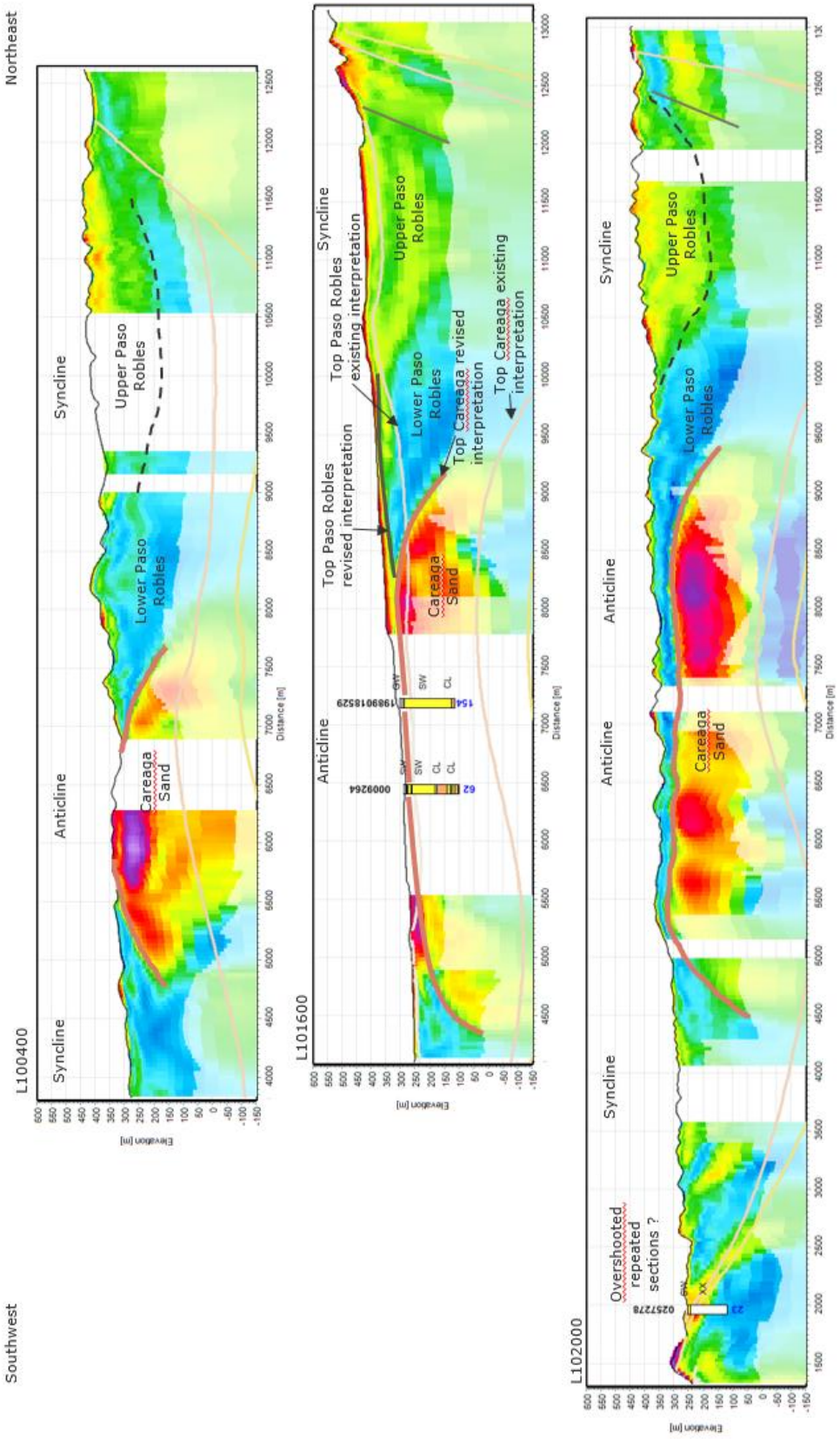

Figure 19 Section L100400, L101600 and L102000.

The vertical sections for line L102400, L106400 and L106600 (see figure XX) are presented on Figure 19. On top of the sections some simple interpretations of faults, synclines, anticlines and interpretations of the geologic formations are made.

On section L106400 and L106600 the thick formation with low resitivities is interpreted to represent the Lower Paso Robles formation. There are very few water bearing layers and the hydraulic connectivity from the NE toward the central part of the basin is deemed to be low. In the central part of the two sections a thick layer of a more horizontal formation is interpreted to represent more coarse quaternary alluvial deposits. At around 6500 m the baseline fault is seen.

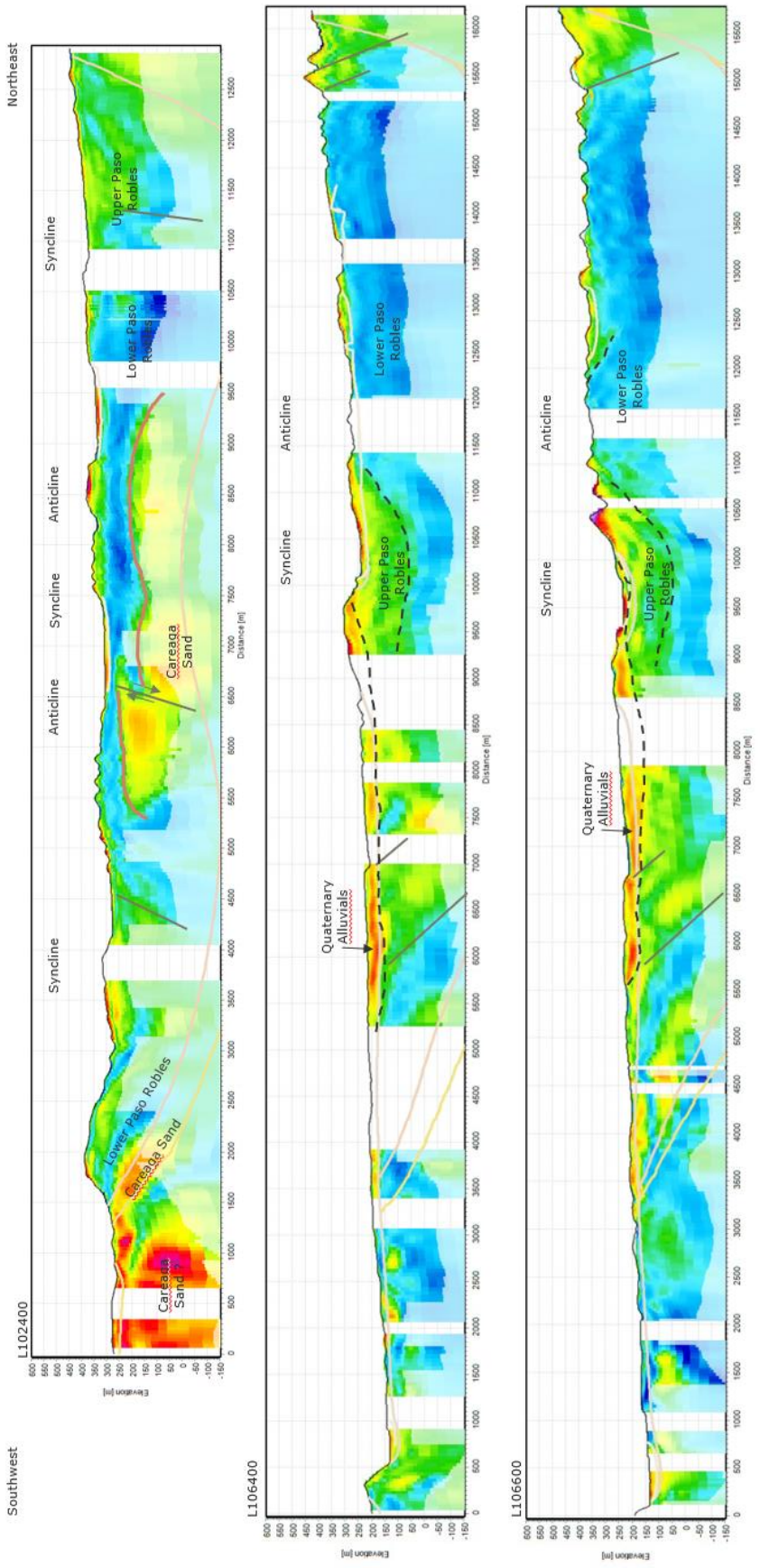

Figure 20 Section L102400, L106400 and L106600.

The vertical sections for line L108800, L110100, L111100 and L111900 (see figure XX) are presented on Figure 21Figure 19. On top of the sections some simple interpretations of faults, synclines, anticlines and interpretations of the geologic formations are made. Within this more southern part of the survey fewer geologic features have been mapped on the surface and very few boreholes are available to support the interpretation.

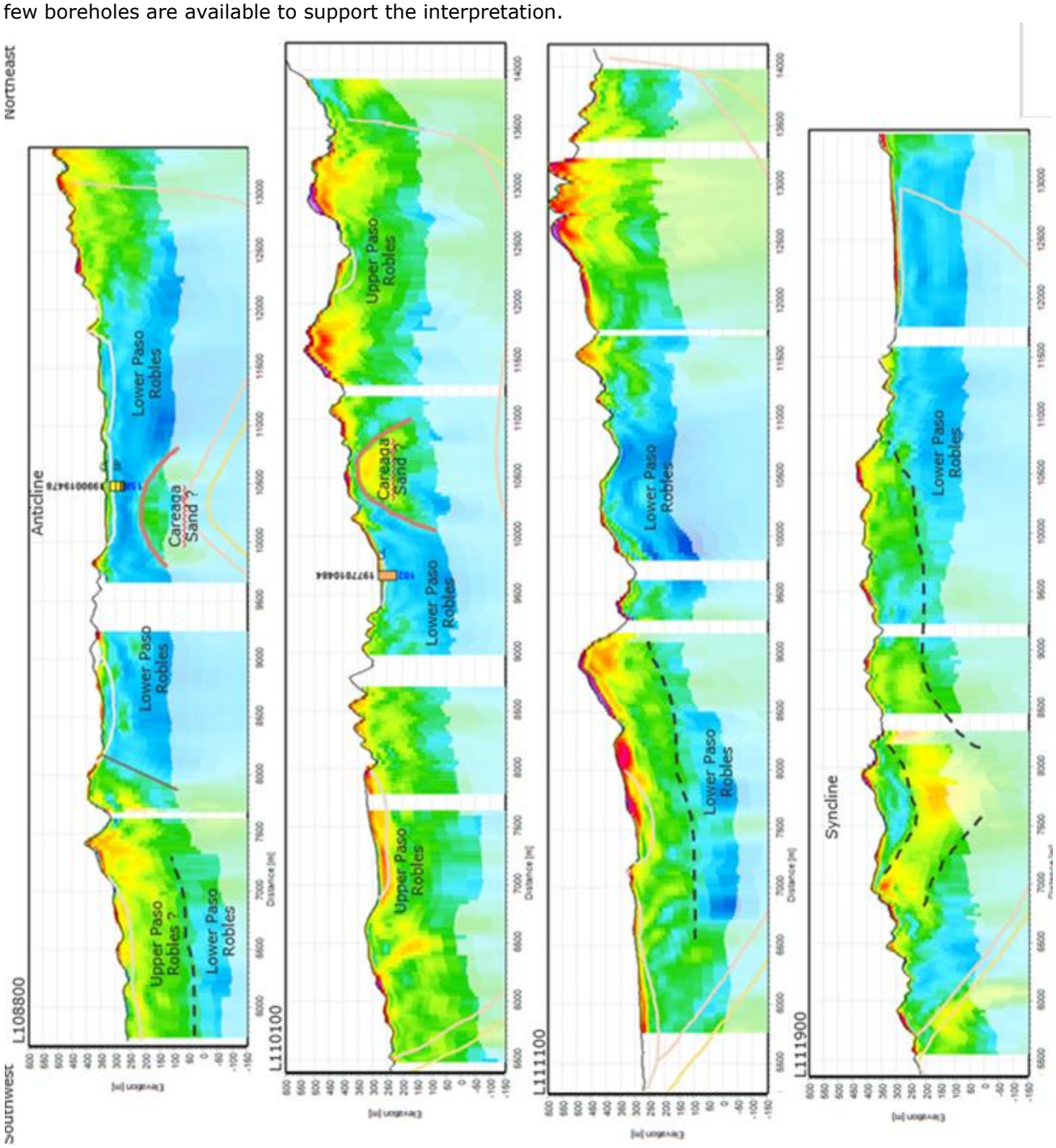

Figure 21 Section L108800, L110100, L111100 and L111900.

7.3.1 The Western Basin Boundary

The basin boundary to the northwest is placed at a topographical water divide. To the west, the San Antonio Creek drains the terrain to the west and east of the basin boundary. The Zaca Creek

drains the area towards south. The water levels in the Careaga Sand and in the Paso Robles Formation indicate that flow will run in parallel with the boundary, both in the shallow and the deeper aquifer. It is worth noting that this is based on information from only three wells in each formation.

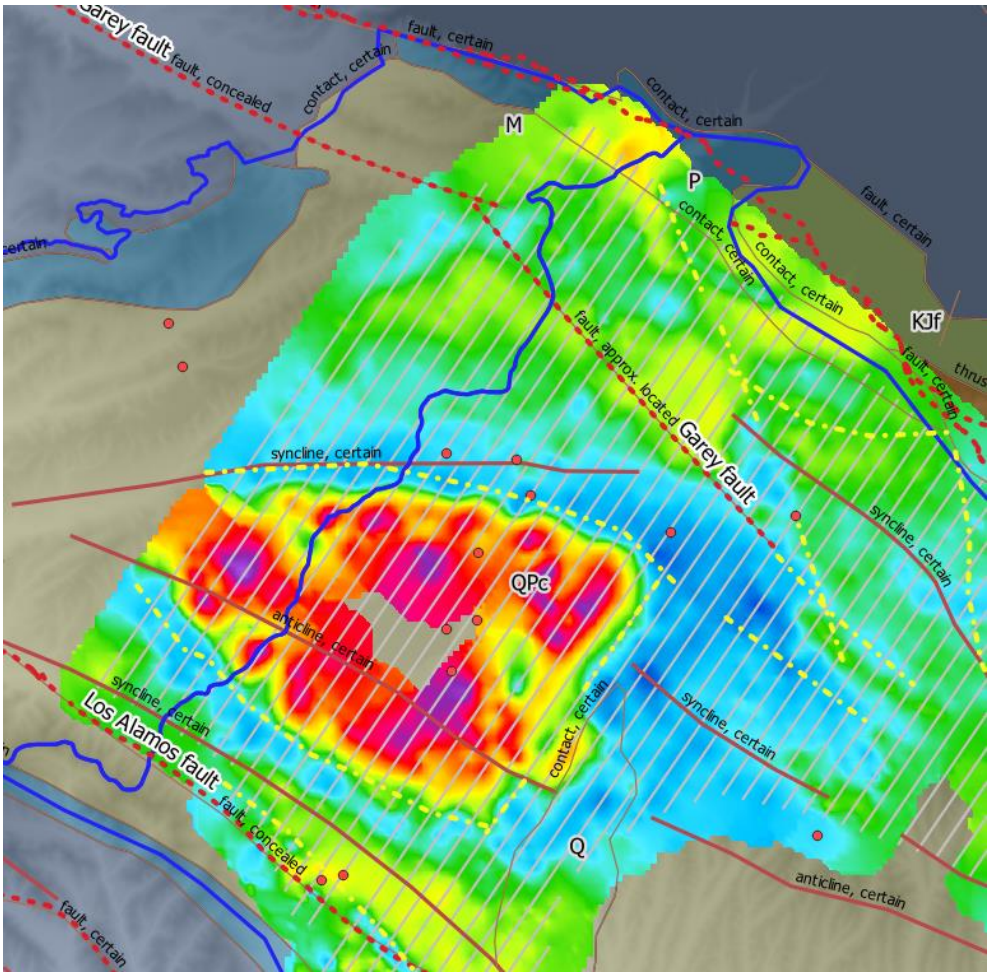

Figure 22 Western boundary of the basin. Resistivities in the elevation interval 240-260 m above mean sea level. Blue line defines the current basin boundary
Figure 23 The Figuero Mountains vertical section by T. W. Dibblee

7.4 Faults, Synclines and Anticlines

The survey area is characterized by a number of faults generally running northwest-southeast; Santa Ynez River Fault Zone, Casmalia Fault, Los Alamos Fault, Baseline Fault, Garey Fault, Little Pine Fault Zone and the Big Pine Fault Zone.

The existing faults correlate well with the variation seen in the electromagnetic data (resistivity images) and the magnetic data (TMI and 1VD grids, See Appendix 7). In addition, the extent of existing fault zones, as well as location of new concealed fault zones have been identified, as shown on the map below (see Figure 24).

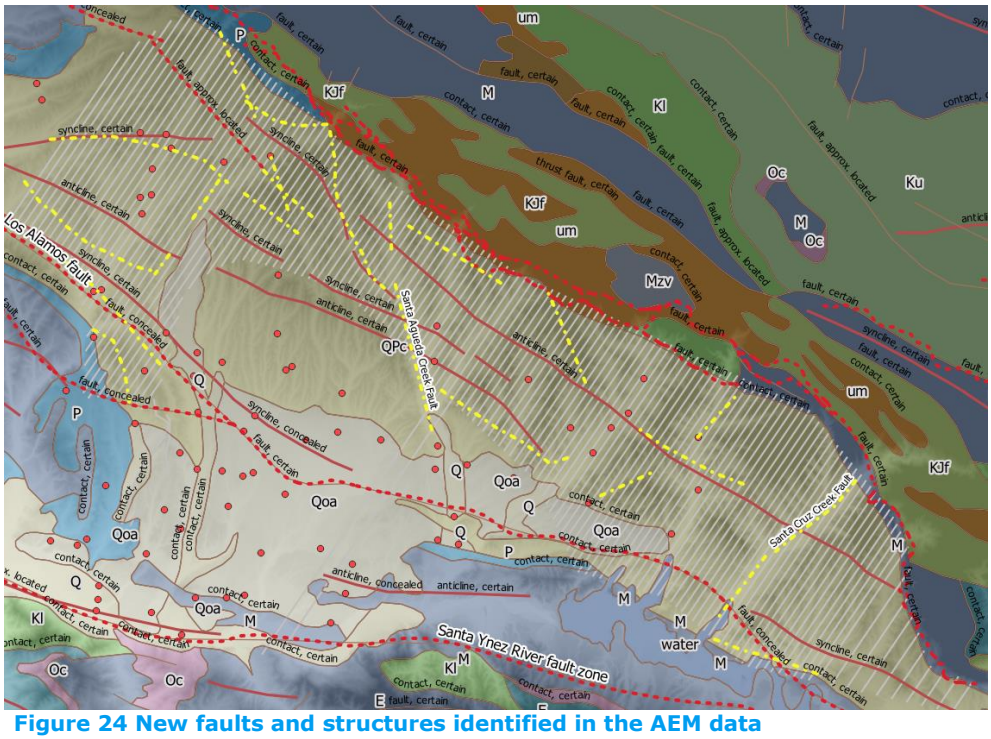

Figure 24 New faults and structures identified in the AEM data

The existing faults are in general based on field observations of outcropping geology as compared to the faults identified in the geophysical data the structures might represent the faults at depth. When the faults do not have a steep dip, there might be an offset in the location of the faults.

8. DATA DELIVERABLES

The project deliverables consist of the following files:

1. **Raw SkyTEM Data**. Raw data as extracted from the instrument, including:
   A. " *.sps " files – Ascii files with information about the geographical coordinates, transmitted current and many other supporting data. The file names start with YYYYMMDD_HHMMSS_MMM and have an extension of ".sps". An additional "*.sps" file contains recorded data at a DGPS base station. The file is named YYYMMDD_##_Base#####_GPS#.
   B. " *.skb " files – Binary data files including recorded electromagnetic decay measurements. These files have an extension of ".skb". The binary file header contains an ascii section with all information about measurement cycles and instrument settings.
   C. " *.lin " files – Ascii files with an extension of ".lin" describe the start and end of each survey line ("…Prod.lin") and the reference lines ("…RefLine.lin").
   D. Geo files – Ascii files with the extensions ".gex" and ".sr2" contain the system description (geometry, waveform, filters etc.).
2. **AEM Database.** A GERDA Firebird database containing all collected data, processed data, as well as the inverted model results. The database can be opened with the software package Aarhus Workbench Viewer.
3. **AEM GIS, Grid, GeoTIF.** ArcGIS layers, grid files and geo-referenced TIF files including:

A. Layout – ArcGIS shape files ("*.shp") containing geographical information about the surveyed area, surveyed flight lines, retained flight lines after data processing, utilities etc.
B. Boreholes – An ArcGIS shape file ("*.shp") containing location of boreholes
C. Mean Resistivity Maps – Geo-referenced TIF files ("*.tif*) illustrating plan-view maps of average resistivities within different elevation intervals that are presented in this report (20-m elevation intervals from 700 m to 0 m a.s.l. Each file name includes information about the top and bottom of the interval.
D. Model Sections – ArcGIS shape files ("*.shp") containing geographical information for the vertical sections presented in this report.

4. **XYZ Model Outputs.** Ascii files with an extension of *.xyz* containing exported models from the GERDA database in two different file formats.
5. **Raw tTEM Data**. Raw data as extracted from the instrument, including:
   E. " *.sps " files – Ascii files with information about the geographical coordinates, transmitted current and many other supporting data. The file names start with YYYYMMDD_HHMMSS_MMM and have an extension of ".sps".
   F. " *.skb " files – Binary data files including recorded electromagnetic decay measurements. These files have an extension of ".skb". The binary file header contains an ascii section with all information about measurement cycles and instrument settings.
   G. " *.lin " files – Ascii files with an extension of ".lin" describe the start and end of each survey line ("…Prod.lin").
   H. Geo files – Ascii files with the extensions ".gex" and ".sr2" contain the system description (geometry, waveform, filters etc.).
6. **tTEM Database.** A GERDA Firebird database containing all collected data, processed data, as well as the inverted model results. The database can be opened with the software package Aarhus Workbench Viewer.
7. **GIS, Grid, GeoTIF.** ArcGIS layers, grid files and geo-referenced TIF files including:
   A. Layout – ArcGIS shape files ("*.shp") containing geographical information about the surveyed area, surveyed flight lines, retained lines after data processing, utilities etc.
   B. Model Sections – ArcGIS shape files ("*.shp") containing geographical information for the vertical sections presented in this report.
8. **XYZ Model Outputs.** Ascii files with an extension of *.xyz* containing exported models from the GERDA database in two different file formats.
9. **Project Report.** A project report is delivered as a PDF document.

The structure of the project digital data delivery folder is shown in

Table 2. In each folder, a text file named “Readme.txt” describes detailed information of the files within the folder.

Table 2 Structure of the project digital data delivery folder.

Folder	Subfolder	Subfolder	Subfolder	File Format	Content
01_Raw_SkyTEM_Data	YYYYMMDD	01_RawData	YYYMMDD.## (flight number)	.sps .skb	Raw data files
		02_Mask		.lin	Production files
		03_Geo		.gex .sr2	System description
02_Database				.gdb	GERDA Firebird Database
03_GIS_Grid_GeoTIFF	01_Layout			.shp	General survey information
	02_Boreholes			.shp	Borehole locations
	03_Mean_Resistivity_Maps			.tif	Mean resistivity plan view maps
	04_Model_Sections			.shp	Locational information of the model sections
04_XYZ_Model_Outputs				.xyz	Exported resistivity models
05_Report				.pdf	Project report

9. CONCLUSIONS AND RECOMMENDATIONS

The geophysical survey provided a detailed three-dimensional resistivity image of the subsurface from the ground surface to approximately 300 m (1,000 ft) depth. Compared to the existing hydrogeologic conceptual model (HCM) the geophysical investigation has revealed that the geology is very complex due to the location in a very active tectonic geographical area. A large number of faults is identified in the geophysical data, of which many of them tie up nicely with faults mapped.

Due to limited accessibility to the Santa Ynez Riverbed very few data were collected here. Accordingly, the coverage of the riverbed was limited, and the outcome of the tTEM survey was not as informative as expected.

The Paso Robles Formation is the dominating geology within the depth of investigation. The existing HCM does not divide the Paso Robles Formation based on intervals with fine and more coarse sediments. It is evident from the AEM model results that the Paso Robles formation can be sub-divided into units that are dominated by finer sediments and other units that are more coarse dominated. In general, it is found that the Paso Robles Formation is more fine-grained in the deeper part and more coarse towards the surface.

In more areas and especially at the Zaca Oil field, it is found that the Careaga Formation is more shallow than described by the existing HCM. The Careaga sand is found to be connected to large anticline structures. The layers on top of the Careaga sand are the more clay dominated sequence of the lower Paso Robles formation; therefore, it is likely that any aquifers hosted in the Careaga sand are hydraulicly disconnected.

The northwestern boundary of the basin is primarily based on a terrain evaluation and the piezometric pressure in a very few boreholes. It is likely that the groundwater flow and hence the boundary of the basin can be modified based on a close examination of the geophysical data and new test boreholes.

Ramboll recommends that the initial interpretations of the tTEM and AEM data made in this report be further developed. This will utilize the large amount of information and details provided by the geophysical investigations to support a future update of the HCM for the basin.

To the north of the Zaca Oil field and along the northern basin boundary, syncline structures filled with more coarse upper Paso Robles sediments are often seen. The hydraulic connectivity towards the south might be reduced due to the folded and faulted clays in the lower Paso Robles Formation.

To make full use of the SkyTEM and tTEM modelling results, further geologic interpretations of the 3D-resistivity results is recommended.

APPENDIX 1
AEM PROCESSING AND INVERSION SETTINGS

APPENDIX 2
TTEM INSTRUMENTATION, PROCESSING AND INVERSION SETTINGS

tTEM INSTRUMENTATION, PROCESSING AND INVERSION SETTINGS

The towed-TEM (tTEM) and WalkTEM instruments are time-domain electromagnetic systems designed for hydrogeophysical and environmental investigations. The instruments were developed based on many years of research at Aarhus University in Denmark. The experience dates back to the development of the pulled-array TEM (PATEM) system and later the SkyTEM airborne system.

tTEM Instrument

This section describes the tTEM instrument, documentation for calibration, results of repeated lines within the survey area and the settings being applied for this specific survey. The information is provided to give an in-depth understanding of the data collection, processing and inversion.

Instrument Setup

The tTEM system measures continuously while towed on the ground. It is designed to provide a very high near-surface resolution with very early time gates and a fast repetition frequency. The tTEM is based on an off-set loop configuration, with the receiver coil (Rx-coil) pulled ~ 8.0 m behind the transmitter coil (Tx-coil). The Rx-coil is horizontal, i.e. measuring the z-component of the magnetic fields. An ATV or similar vehicle tows the tTEM-system. The distance between the ATV and the Tx coil is 3.0 m. The Tx-coil is a 2 m x 4 m loop suspended by the red beams, as shown on the photo in Figure A2-1. A GPS is located at the front of the Tx-frame for accurate positioning of the system. The Rx-coil is placed on a small sled. The transmitter electronics, receiver instrument, power supply etc. are carried on the back of the ATV.

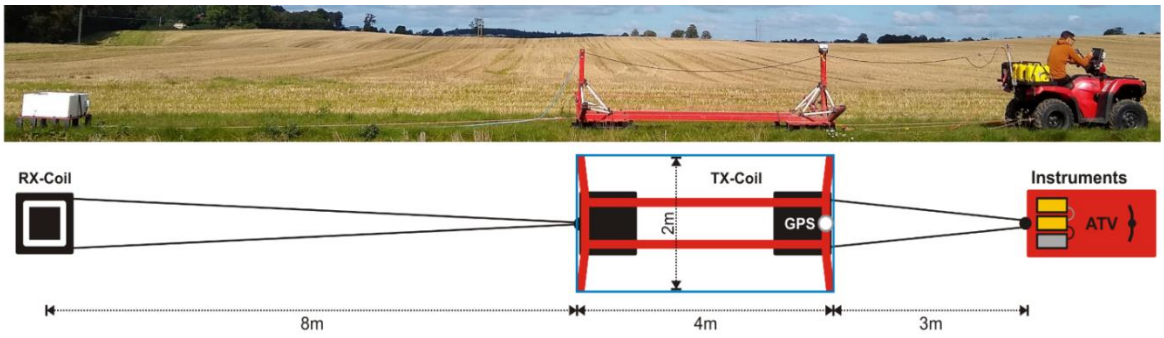

Figure A2- 1 The tTEM system configuration.

tTEM Instrument IDs

For this survey, the instruments with ID's shown in Table A2- 1 were used.

Unit	ID1	ID2
TIB Receiver instrument	13	20180843
RC20 Receiver coil		20200217
tTEM Transmitter	TX11	20200209
Novatel Agstar GPS		20200640

Table A2- 1 ID's for the instrumentation used in this survey.

Device Positions, Nominal

The positions and the geometry of the main components are listed in Table A2- 2 and used in the processing and inversion scheme. As an example, the GPS coordinate is measured in the front of the transmitter frame, and then during the processing of the GPS data, the coordinates are shifted to reflect the actual focus point of the system. The geometry of the transmitter frame and the exact off-set of the receiver coil are used during the inversion of the data.

Unit	X (m)	Y (m)	Z(m)
GP_Tx (GPS)	2.00	0.00	-1.20
RxZ (Z-receiver coil)	-10.28	0.00	-0.30
Tx-Coil, center	0.00	0.00	-0.50
Tx-Coil corner 1	-2.00	-1.00	-0.50
Tx-Coil corner 2	2.00	-1.00	-0.50
Tx-Coil corner 3	2.00	1.00	-0.50
Tx-Coil corner 4	-2.00	1.00	-0.50

Table A2- 2 Nominal equipment, receiver and transmitter coils positioning. The origin is defined as the center of the transmitter coil. Z is positive downwards.

Transmitter Waveform

The current in the transmitter loop is turned on and off in pulses. The direction of the current shifts from positive to negative in between each pulse. The two graphs below show the waveform for the low moment (LM) and the high moment (HM) as the current is turned off very rapidly. During the off times, i.e. when the current is turned off, the secondary magnetic fields from the eddy currents are measured in the receiver coil.

Figure A2- 2 Close-up photo showing the transmitter frame mounted on the sled

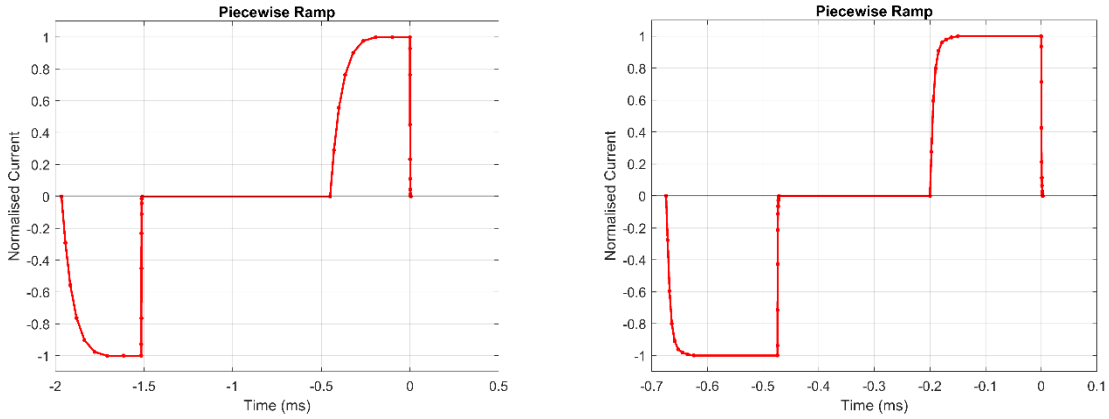

Figure A2- 3 Waveforms for the LM (left) and the HM (right). The red line segments indicate the piecewise linear modelling of the waveforms.

The speed of the turn-off ramp of the low moment is critical for the resolution of the shallow subsurface. Table A2- 4 shows a closeup view of the ramp down on the low moment; the current is turned off within approximately 2 microsecond (µS).

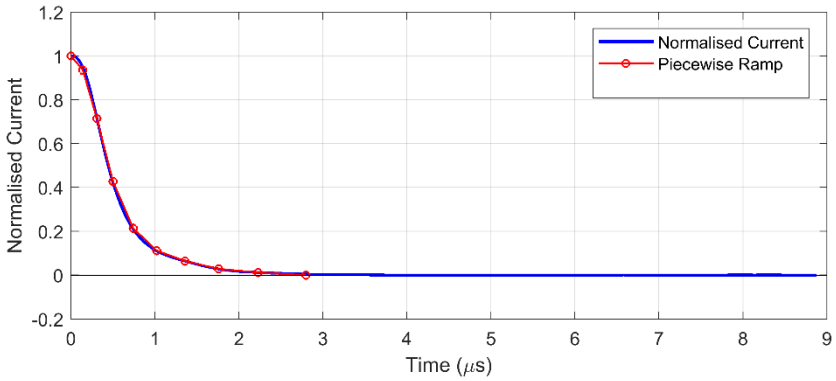

Figure A2- 4 Close-up on ramp down for LM. The red line segments indicate the piecewise linear modelling of the waveform.

The transmitter waveforms for LM and HM, are listed as time and nominal amplitude. On-times are negative, and off-times are positive. The shape of the waveform is used in the inversion scheme. The actual waveforms are scaled by the current measurement just before the current is turned off.

LM time	LM amplitude	HM time	HM amplitude
-6.7400e-04 s	-0.000	-1.9650e-03 s	-0.000
-6.7250e-04 s	-0.496	-1.9483e-03 s	-0.316
-6.7071e-04 s	-0.658	-1.9279e-03 s	-0.532
-6.6859e-04 s	-0.784	-1.9030e-03 s	-0.710
-6.6605e-04 s	-0.865	-1.8725e-03 s	-0.845
-6.6303e-04 s	-0.925	-1.8351e-03 s	-0.933
-6.5944e-04 s	-0.963	-1.7894e-03 s	-0.981
-6.5516e-04 s	-0.978	-1.7334e-03 s	-1.001
-6.5007e-04 s	-0.989	-1.6650e-03 s	-1.000
-6.4400e-04 s	-1.000	-1.5150e-03 s	-1.000
-4.7400e-04 s	-1.000	-1.5148e-03 s	-0.967
-4.7387e-04 s	-0.953	-1.5146e-03 s	-0.859
-4.7373e-04 s	-0.812	-1.5143e-03 s	-0.662
-4.7355e-04 s	-0.559	-1.5139e-03 s	-0.381
-4.7334e-04 s	-0.332	-1.5135e-03 s	-0.155
-4.7309e-04 s	-0.175	-1.5131e-03 s	-0.053
-4.7279e-04 s	-0.086	-1.5125e-03 s	-0.017
-4.7243e-04 s	-0.041	-1.5118e-03 s	-0.007
-4.7200e-04 s	-0.016	-1.5110e-03 s	-0.000
-4.7150e-04 s	-0.000	-4.5000e-04 s	0.000
-2.0000e-04 s	0.000	-4.3333e-04 s	0.316
-1.9850e-04 s	0.496	-4.1294e-04 s	0.532
-1.9671e-04 s	0.658	-3.8799e-04 s	0.710
-1.9459e-04 s	0.784	-3.5745e-04 s	0.845
-1.9205e-04 s	0.865	-3.2009e-04 s	0.933
-1.8903e-04 s	0.925	-2.7438e-04 s	0.981
-1.8544e-04 s	0.963	-2.1844e-04 s	1.001
-1.8116e-04 s	0.978	-1.5000e-04 s	1.000
-1.7607e-04 s	0.989	0.0000e+00 s	1.000
-1.7000e-04 s	1.000	2.0384e-07 s	0.967
0.0000e+00 s	1.000	4.3584e-07 s	0.859
1.2589e-07 s	0.953	7.2384e-07 s	0.662
2.6989e-07 s	0.812	1.0598e-06 s	0.381
4.5389e-07 s	0.559	1.4598e-06 s	0.155
6.6189e-07 s	0.332	1.9398e-06 s	0.053
9.0989e-07 s	0.175	2.5078e-06 s	0.017
1.2139e-06 s	0.086	3.1878e-06 s	0.007
1.5659e-06 s	0.041	4.0000e-06 s	0.000
1.9979e-06 s	0.016		
2.8000e-06 s	0.000		

Table A2- 3 Transmitter waveforms LM and HM.

Measurement Cycle

The basic settings of the instrumentation are shown in Table A2- 4.

Parameter	LM	HM
Moment ID	2	1
No. of turns	1	1
Transmitter area (m2)	8 m2	8 m2
Tx Current	~ 3 A	~ 30 A
Tx Peak moment	~ 24 Am2	~ 240 Am2
Repetition frequency	1008 Hz	282 Hz
Raw Data Stack size	366	282
Raw Moment cyclus time	0.22 s	0.40 s
Tx on-time	200 µs	450 µs
Duty cycle	42%	30%
Turn-off time	2.6 µs at 3 Amp	4.5 µs at 30 Amp
Number of gates	5	25
Gate time interval (gate center time)	4 µs – 30 µs	10 µs – 900 µs
Front-gate time (nominal)	2 µs	4 µs
Front-gate delay	2 µs	2 µs

Table A2- 4 Basic settings of the instrumentation.

Receiver Coil

The receiver coil can be described by the following parameters. The parameters are used in the inversion scheme.

Parameter	Value
Low pass filter frequency	300 kHz
Low pass filter order	1
Effective area	20m^2

Table A2- 5 Receiver coil parameters.

Instrument Firmware Versions

The firmware in the instruments have the version numbers described in the table below.

Software	Version
PaPC	4.1.1.8
Navsys	2.1.0.4
TxProc	2.10.0.30
tTEM Log	5.0.4.8
NAV	5.2.0.2

Table A2- 6 Instrument firmware versions.

Documentation of Test and Calibration

At the Danish national geophysical test-site near Aarhus, Denmark, the tTEM instrumentation described above was tested and calibrated. The purpose for the test and calibration is to document the performance of the instrument and to defined absolute calibration parameters.
The calibration is performed to establish the absolute time shift and data level to facilitate precise modeling of the data. No additional levelling or drift corrections are applied. To perform the calibration, all system parameters (transmitter waveform, low pass filters, etc.) must be known to allow accurate modeling of the tTEM setup. The calibration constants are determined by comparing a recorded tTEM response on the test site with the reference response. The reference response is calculated from the test site reference model for the used tTEM configuration.

Acceptable calibration was achieved with the calibration constants stated in Table A2- 7. The calibration was performed on June 9, 2019. Calibration plots for both moments are shown in Figure A2- 5 and Figure A2- 6. The scale factors of 1.01 and 1.03 (1% and 3%) are very acceptable. The time shift is deemed due to the delays in the electronics and inaccurately modelled waveforms. The obtained time shifts are very acceptable.

Moment	Time Shift	Scale Factor
LM	-0.80 µs	1.01
HM	-0.70 µs	1.03

Table A2- 7 Calibration constants.

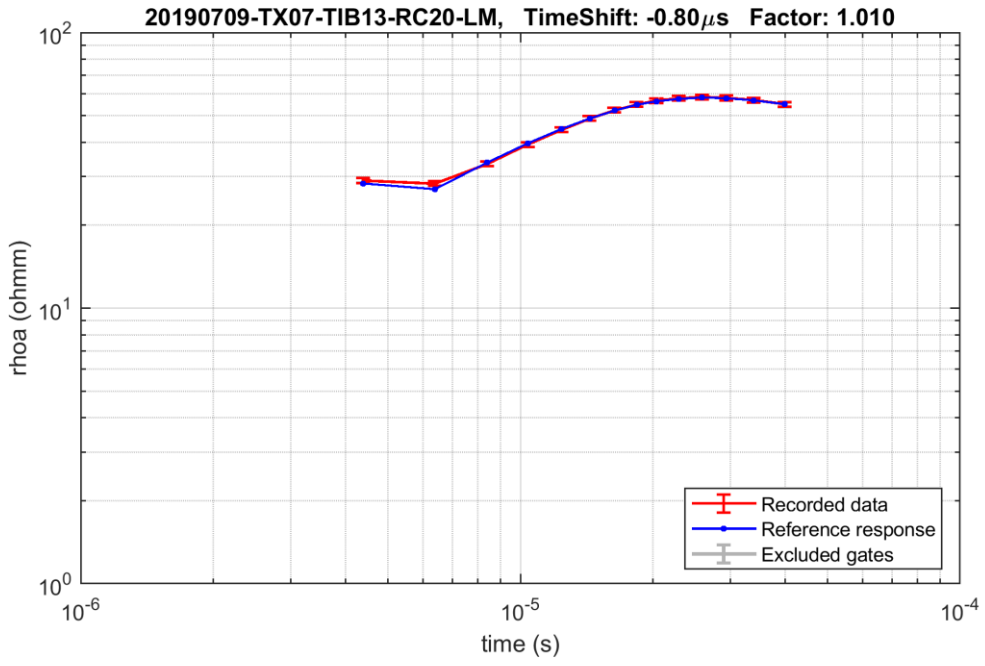

Figure A2- 5 Calibration plot for the LM. The red curve is the recorded data with calibration factors applied, and the blue curve is the forward response from the national geophysical test-site in Denmark.

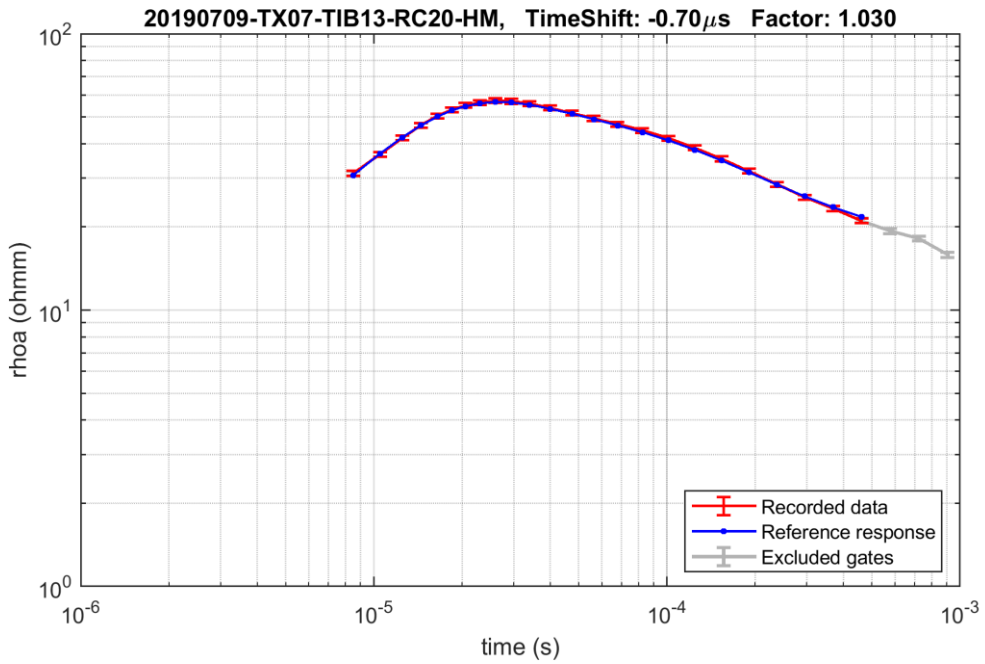

Figure A2- 6 Calibration plot for the HM. The red curve is the recorded data with calibration factors applied, and the blue curve is the forward response from the national geophysical test-site in Denmark.

Processing and Inversion Software Settings

The processing and inversion are based on the Aarhus Workbench software, version 6.4.0.0. A 30-layer model has been applied. Table A2- 8 **Outline of the 25-layer model.** lists the fixed layer thicknesses, depth to bottom of layer and the initial resistivity assigned to the model layers (a homogenous half space). For this survey, the initial resistivity values were obtained by first inverting each tTEM sounding data with homogeneous half-space earth model and the resulting values were used during the inversion.

Layer	Thickness [Meter]	Depth [Meter]	Start value [Ohm-m]
1	1.00	1.00	Auto
2	1.10	2.10	Auto
3	1.20	3.20	Auto
4	1.30	4.50	Auto
5	1.30	5.80	Auto
6	1.50	7.30	Auto
7	1.60	8.90	Auto
8	1.70	10.6	Auto
9	1.80	12.4	Auto
10	2.00	14.3	Auto
11	2.10	16.5	Auto
12	2.30	18.7	Auto
13	2.50	21.2	Auto
14	2.60	23.8	Auto

Layer	Thickness [Meter]	Depth [Meter]	Start value [Ohm-m]
15	2.90	26.7	Auto
16	3.10	29.8	Auto
17	3.30	33.1	Auto
18	3.60	36.7	Auto
19	3.90	Auto.5	Auto
20	4.20	44.7	Auto
21	4.50	49.1	Auto
22	4.80	53.9	Auto
23	5.20	59.1	Auto
24	5.60	64.7	Auto
25	6.00	70.8	Auto
26	6.50	77.3	
27	7.00	84.3	
28	7.60	91.9	
29	8.10	100	
30	--		

Table A2- 8 Outline of the 25-layer model.

GPS Settings

The settings and the position of the GPS is shown in Table A2- 9.

Parameter	Value
Beat Time	0.5 sec
Filter length	7.0 sec
Polynomial order	2
Shift in x-direction	-4.965 m

Table A2- 9 GPS processing.

APPENDIX 3
AEM MEAN RESISTIVITY MAPS – 20 METER ELEVATION INTERVALS

APPENDIX 4
AEM QC MAPS – RESIDUAL, DOI, NO DATAPOINT, TX HEIGHT

APPENDIX 5
AEM VERTICAL SECTIONS

APPENDIX 6
COMPARISON OF AEM MODELS WITH LITHOLOGIC INFORMATION

A total of 14 wells the lithology has been digitized and

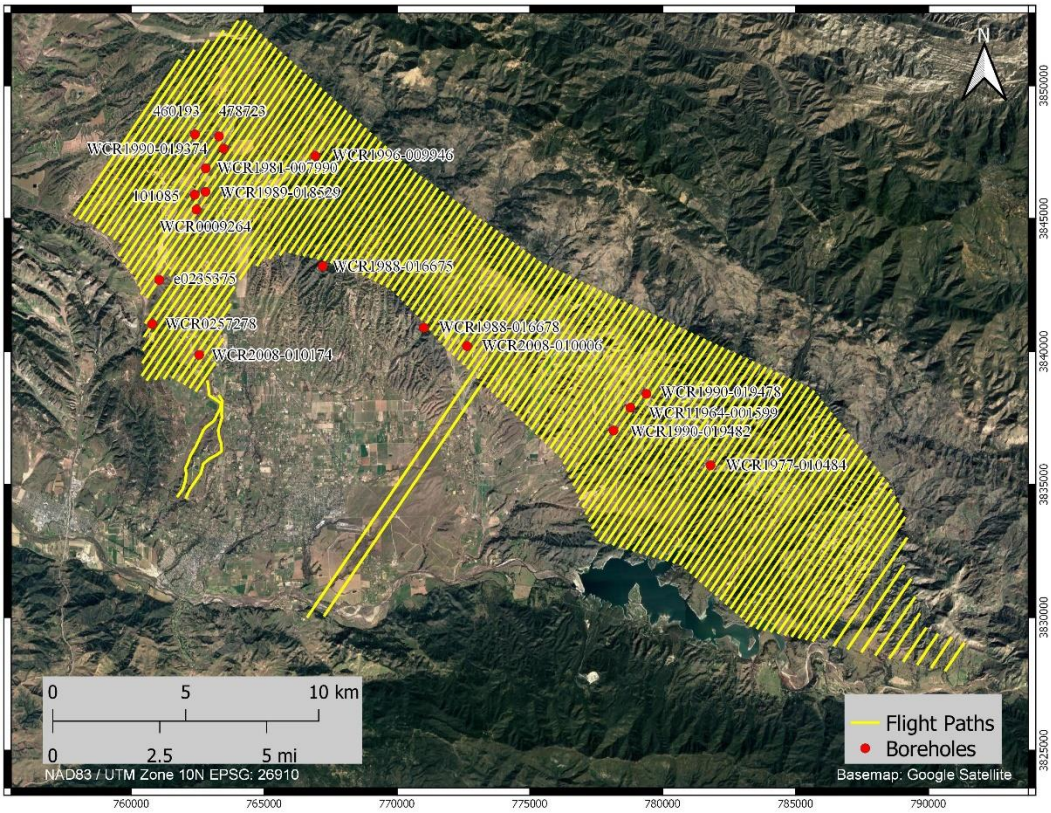

The figure shows the location of the boreholes in the survey area with a good lithological description, that has been used for a direct comparison to the AEM sections.

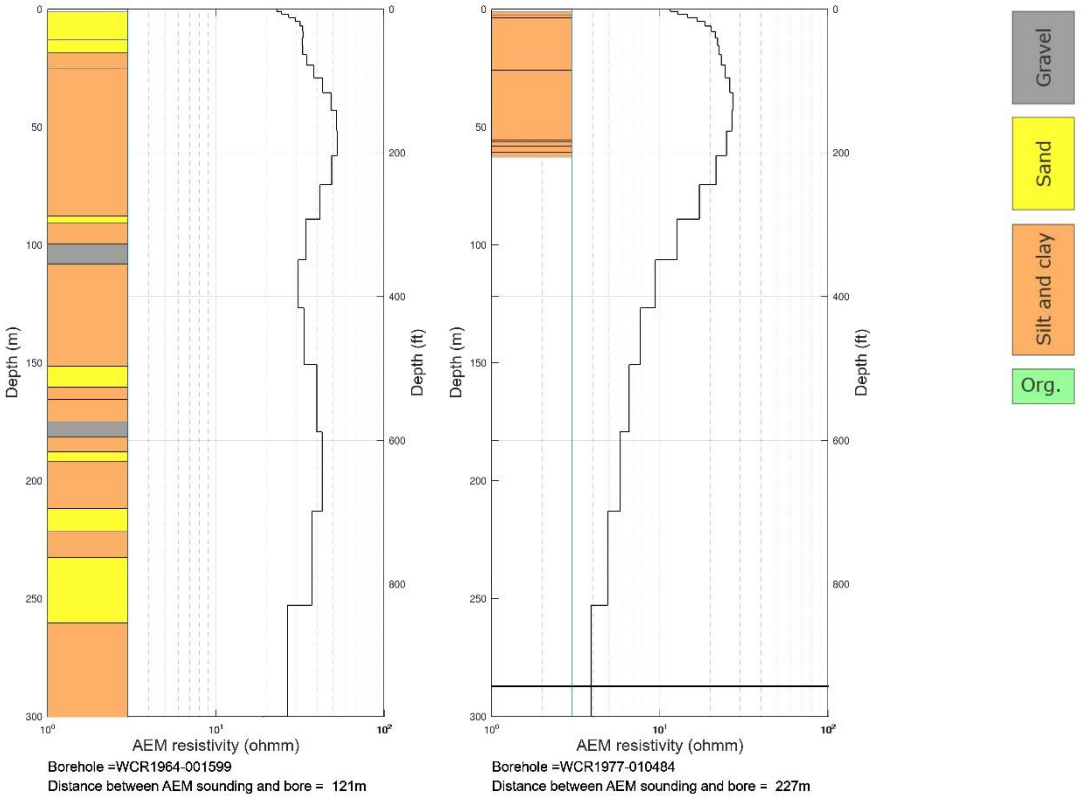
Depth (m)
Depth (ft)
AEM resistivity (ohmm)
Borehole =WCR1964-001599
Distance between AEM sounding and bore = 121m
Borehole =WCR1977-010484
Distance between AEM sounding and bore = 227m
Gravel
Sand
Silt and clay
Org.

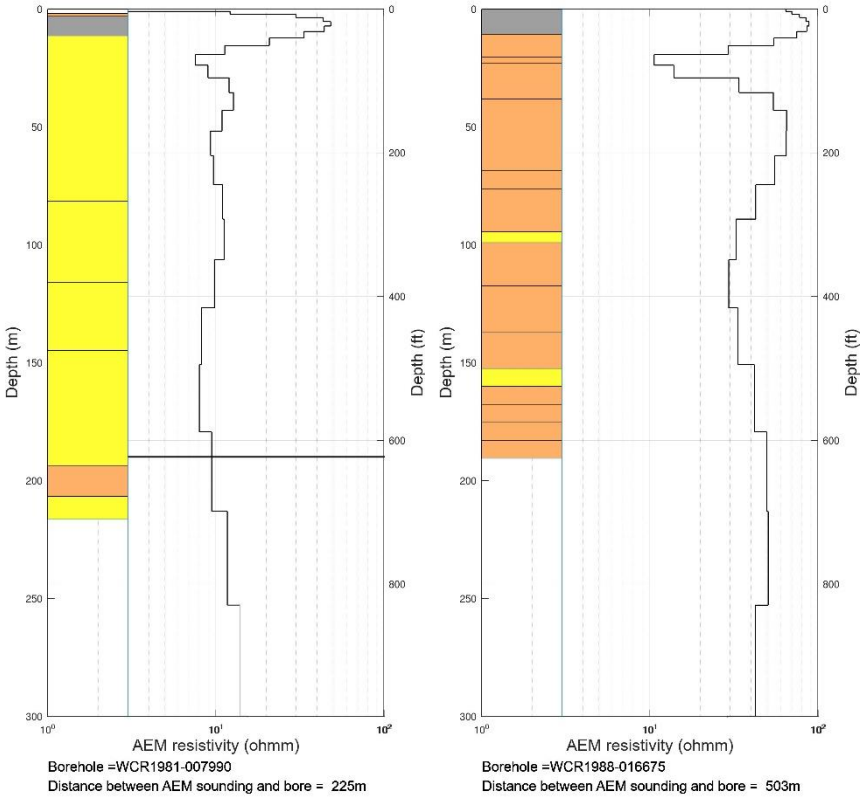
Depth (m)
Depth (ft)
AEM resistivity (ohmm)
Borehole =WCR1981-007990
Distance between AEM sounding and bore = 225m
Depth (m)
Depth (ft)
AEM resistivity (ohmm)
Borehole =WCR1988-016675
Distance between AEM sounding and bore = 503m

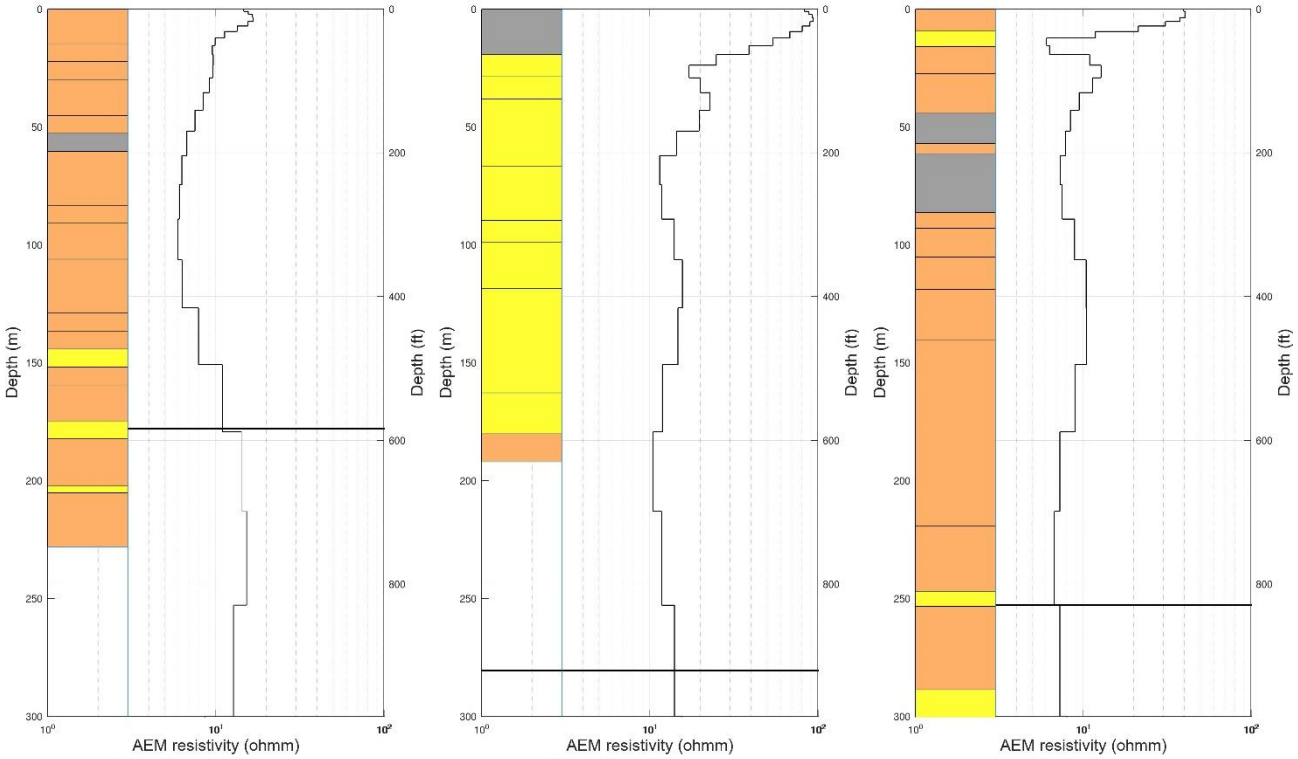
Depth (m)
Depth (ft)
AEM resistivity (ohmm)
Borehole =WCR1988-016678
Distance between AEM sounding and bore = 73m
Borehole =WCR1989-018529
Distance between AEM sounding and bore = 123m
Borehole =WCR1990-019374
Distance between AEM sounding and bore = 5m

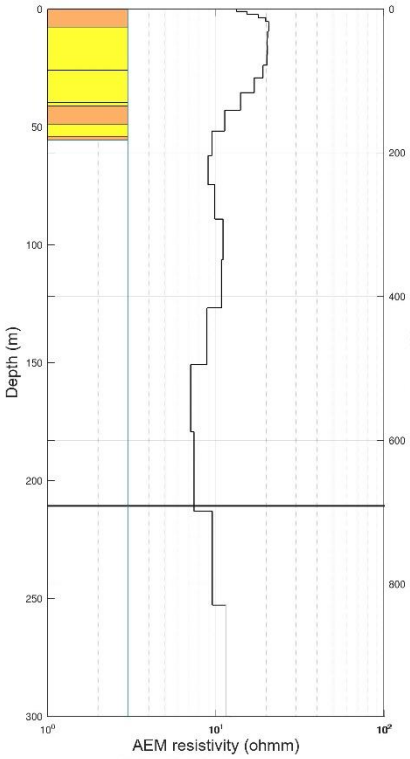

Borehole =WCR1990-019478
Distance between AEM sounding and bore = 141m

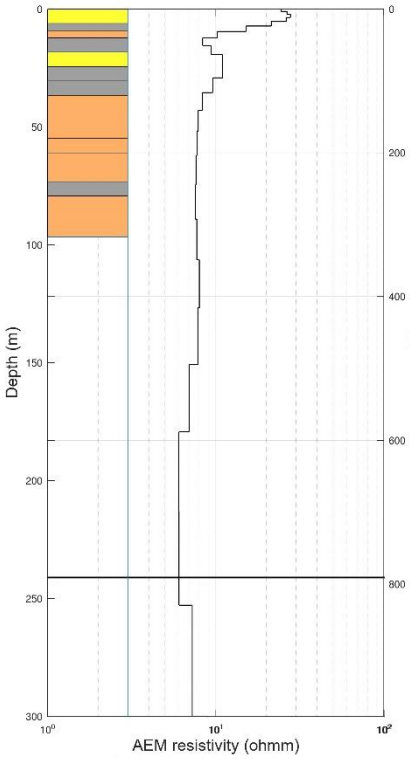

Borehole =WCR1996-009946
Distance between AEM sounding and bore = 102m

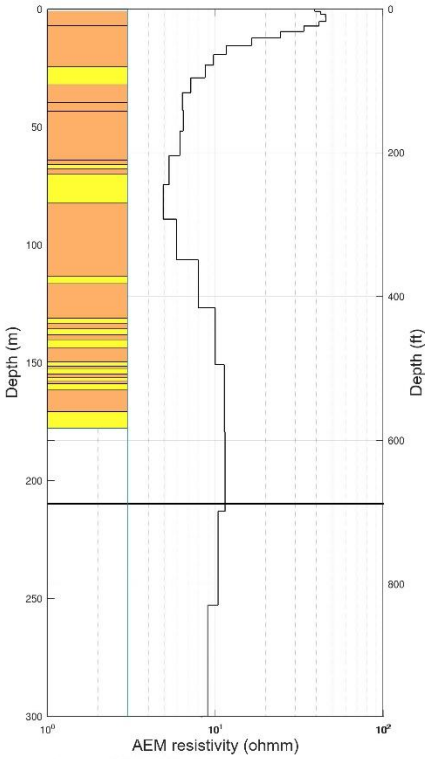

Borehole =WCR2008-010006
Distance between AEM sounding and bore = 89m

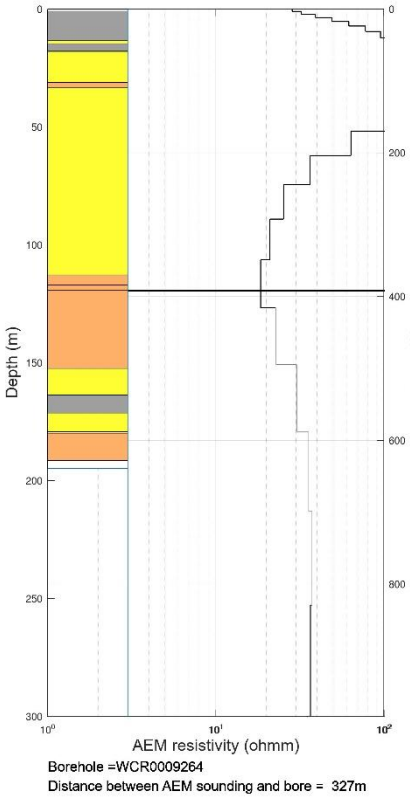

Borehole =WCR0009264
Distance between AEM sounding and bore = 327m

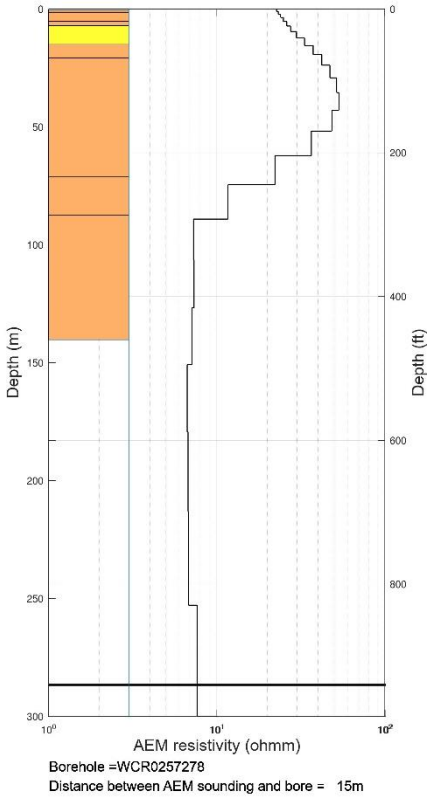

Borehole =WCR0257278
Distance between AEM sounding and bore = 15m

APPENDIX 7
MAGNETIC MAPS

APPENDIX 8
SKYTEM RAW DATA REPORT

APPENDIX 9
TEM INTRODUCTION AND THEORY

TEM INTRODUCTION AND THEORY

Since acquiring the first TEM instrument in the early 1990's, Ramboll has been among the global pioneers when it comes to using TEM soundings for subsurface mapping. Over the last 20 years, the accuracy of the instruments and the ability to obtain information about aquifers and hydrogeological properties has improved significantly. The TEM technique is now one of the most efficient geophysical technologies for groundwater investigations.

Within the last 15 years, the development of airborne TEM systems has provided the possibility to survey large areas in a relatively short time frame as well as to survey in areas that otherwise are logistically challenging.

The development of the land based towed TEM (tTEM) system, is one of the newest additions to the variety of TEM systems available, and it is basically a downscaled version of the airborne SkyTEM time domain electromagnetic system.

TEM Theory

Time domain electromagnetic methods are based on the principle of inducing eddy currents in the ground. A direct current is emitted in a transmitter loop, and when the current stabilizes, the transmitter is abruptly turned off and thereby inducing an electrical field and a current in the ground which results in a secondary magnetic field. A receiver coil located in the center of the transmitter loop (central loop configuration) or outside the transmitter loop (off-set configuration), measures the decaying magnetic field with time. The measured signal will at early times reflect resistivities of near surface layers, while later times will contain information of the resistivities of deeper layers.

Noise in TEM data

TEM data are comprised of different type of noise components. Noise can cause bias signals and affect the depth of investigation and if not properly identified and removed, it can result in incorrect geological and hydrological interpretations. The different sources of noise are described below:

1. A galvanic coupling is caused by the electromagnetic signal being induced in a metal object, such as a metal pipe, metal fence or the loop, following the ground-wire through the power-masts to the ground as sketched below. The challenge is that the signal component caused by a galvanic coupling can be hard to detect as the nature of the decay is similar to the response from the ground as illustrated in the Figure below.

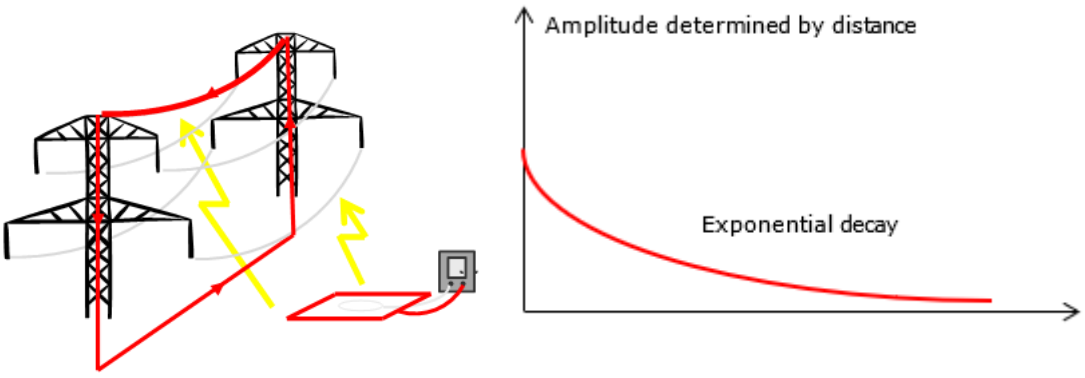

Figure Illustration showing the effects of galvanic coupling on TEM.

2. Capacitive coupling is caused by the electromagnetic signal being induced in an insulated installation such as a power cable. The noise creates an oscillating signal as illustrated in the Figure below. It is generally relatively easy to distinguish a capacitive coupling from a signal caused by the subsurface.

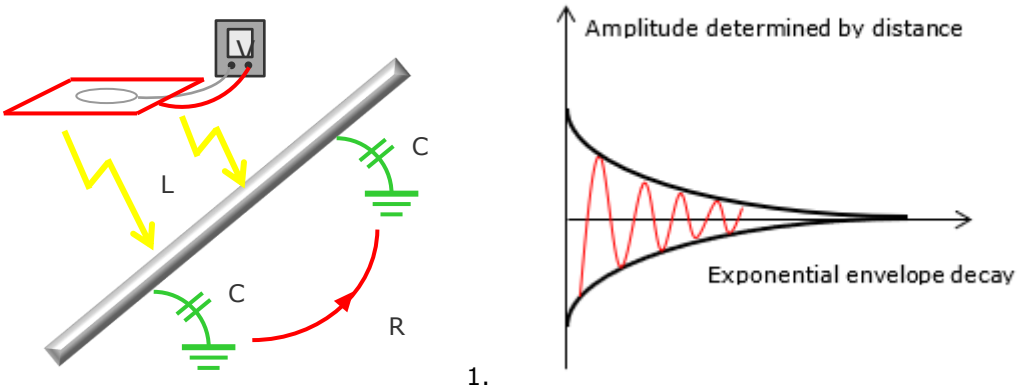

1.

Figure Illustration showing the effects of capacitive coupling.

3. Coherent noise from electrical powerlines has the same pattern as sketched for the capacitive coupling. It is often easy to identify during the processing of the data.

4. Atmospheric noise is more random in nature and is typically handled by none-spike filtering and by simple averaging of the data. In case of strong lightning or an electromagnetic storm during survey acquisition the background noise can prevent the collection of data with a satisfactory signal-to-noise ratio.

5. Motion induced noise due to vibrations in the receiver coil in the earth's magnetic field will create a noise component. This is only problematic for systems which acquire data continuously while being moved, such as airborne systems or e.g. the tTEM system. It is handled by suspending the receiver coil and by keeping the survey speed within specifications.

6. Internal noise in the instrumentation.

Inversion

The inversion of electromagnetic data is the process of fitting the measured electromagnetic responses to the forward responses obtained from a geophysical model described by layers and electrical resistivities. The resulting model is a smooth coherent resistivity model along the inverted survey line.

Thematic Maps and Cross Sections

To visualize the resistivity structures in the mapping area, a number of geophysical maps and cross sections have been created. Furthermore, a location map and a number of maps made for quality control (QC-maps) are found in the appendices.

To make depth or horizontal slices, the mean resistivity in the depth or elevation intervals is calculated for each resistivity model and then interpolated to a regular grid.

Figure 25 shows how the resistivity's of the layers in a model influence the calculation of the mean resistivity in a depth interval [A, B]. d_0 is the surface, d_1, d_2 and d_3 are the depths to the layer boundaries in the model. ρ_1, ρ_2, ρ_3 and ρ_4 are the resistivity's of the layers.

The model is subdivided into sub-thicknesses $\Delta t_{1\text{-}3}$. The mean resistivity (ρ_{vertical}) is calculated as:

$$\rho_{vertical} = \frac{\rho_1 \cdot \Delta t_1 + \rho_2 \cdot \Delta t_2 + \rho_3 \cdot \Delta t_3}{\Delta t_1 + \Delta t_2 \cdot \Delta t_3}$$

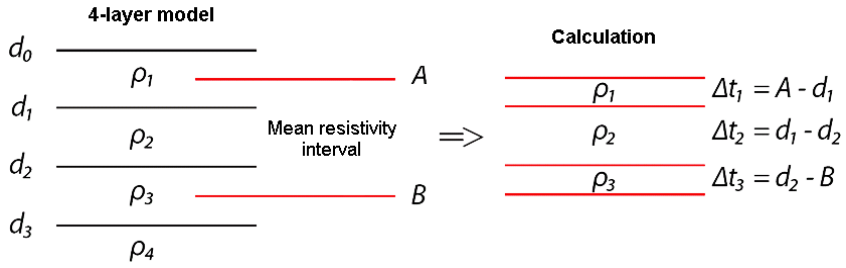

Figure 25 The figure illustrates how the resistivity's of the layers influence the mean resistivity's in a depth interval [A:B]

In the general term the mean resistivity's in a depth interval is calculated using the equation below:

$$\bar{\rho} = \frac{\sum_{i=1}^{n} \rho_i \cdot \Delta t_i}{\sum_{i=1}^{n} \Delta t_i}$$

where i runs through the interval from 1 to the number of sub-thicknesses. The mean resistivity calculated by the above formula (ρvertical) is named the vertical mean resistivity - equal to the total resistance if a current flow vertically through the interval.

By mapping with a TEM method, the current flows only horizontally in the ground. It is therefore more correct to perform the mean resistivity calculation in conductivity in the space, then named the horizontal mean resistivity (ρhorizontal). The horizontal mean resistivity is equal to the reciprocal of the mean conductivity (σmean) and is calculated as:

$$\rho_{horizontal} = \frac{1}{\sigma_{mean}} = \left[\frac{\sum_{1=1}^{n}\left(\frac{1}{\rho_i}\right) \cdot \Delta t_i}{\sum_{i=1}^{n} \Delta t_i}\right]^{-1}$$

For this survey, horizontal mean resistivity themes have been generated from the smooth model inversion result in 10 m depth intervals from 0 to 100 m, and in 20 m intervals from 100 to 450 m. The resistivity models have been blanked at the DOI standard value prior to the interpolation regular mean resistivity grids.

The interpolation of the mean resistivity values to regular grids is performed by Kriging interpolation (Pebesma and Wesseling, 1998), with a node spacing of 50 m and a search radius of 1000 m, and with additional pixel smoothing in the presented bit-maps images.